8. Laser Spectroscopy of Collision Processes

The two main sources of information about atomic and molecular structure and interatomic interactions are provided by spectroscopic measurements and by the investigation of elastic, inelastic, or reactive collision processes. For a long time these two branches of experimental research developed along separate lines without a strong mutual interaction. The main contributions of classical spectroscopy to the study of collision processes have been the investigations of collision-induced spectral line broadening and line shifts (Sect. 3.3).

The situation has changed considerably since lasers were introduced to this field. In fact, laser spectroscopy has already become a powerful tool for studying various kinds of collision processes in more detail. The different spectroscopic techniques presented in this chapter illustrate the wide range of laser applications in collision physics. They provide a better knowledge of the interaction potentials and of the different channels for energy transfer in atomic and molecular collisions, and they give information that often cannot be adequately obtained from classical scattering experiments without lasers.

The high spectral resolution of various Doppler-free techniques discussed in Chaps. 2–4 has opened a new dimension in the measurement of collisional line broadening. While in Doppler-limited spectroscopy small line-broadening effects at low pressures are completely masked by the much larger Doppler width, Doppler-free spectroscopy is well suited to measure line-broadening effects and line shifts in the kilohertz range. This allows detection of *soft collisions* at large impact parameters of the collision partners that probe the interaction potential at large internuclear separations and that contribute only a small line broadening.

Some techniques of laser spectroscopy, such as the method of separated fields (*optical Ramsey fringes*, Sect. 9.4), coherent transient spectroscopy (Sect. 7.5), or polarization spectroscopy (Sect. 2.4) allow one to distinguish between phase-changing, velocity-changing, or orientation-changing collisions.

The high *time resolution* that is achievable with pulsed or mode-locked lasers (Chap. 6) opens the possibility for studying the dynamics of collision processes and relaxation phenomena. The interesting questions of how and how fast the excitation energy that is selectively pumped into a polyatomic molecule by absorption of laser photons, is redistributed among the various degrees of freedom by intermolecular or intramolecular energy transfer can be addressed by femtosecond laser spectroscopy.

One of the attractive goals of laser spectroscopy of reactive collision processes is the basic understanding of chemical reactions. The fundamental question in laser chemistry of how the excitation energy of the reactants influ-

ences the reaction probability and the internal state distribution of the reaction products can, at least partly, be answered by detailed laser-spectroscopic investigations. Section 8.4 treats some experimental techniques in this field.

The most detailed information on the collision process can be obtained from laser spectroscopy of *crossed-beam* experiments, where the initial quantum states of the collision partners before the collision are marked, and the scattering angle as well as the internal energy of the reactants is measured. In such an "ideal scattering experiment" all relevant parameters are known (Sect. 8.5).

The new and interesting field of *light-assisted collisions* (often called optical collisions), where absorption of laser photons by a collision pair results in an effective excitation of one of the collision partners, is briefly treated in the last section of this chapter. For further studies of the subject covered in this chapter, the reader is referred to books [8.1–8.3], reviews [8.4–8.10], and conference proceedings [8.11–8.14].

8.1 High-Resolution Laser Spectroscopy of Collisional Line Broadening and Line Shifts

In Sect. 3.3. we discussed how elastic and inelastic collisions contribute to the broadening and shifts of spectral lines. In a semiclassical model of a collision between partners A and B, the particle B travels along a definite path $\boldsymbol{r}(t)$ in a coordinate system with its origin at the location of A. The path $\boldsymbol{r}(t)$ is completely determined by the initial conditions $\boldsymbol{r}(0)$ and $(\mathrm{d}\boldsymbol{r}/\mathrm{d}t)_0$ and by the

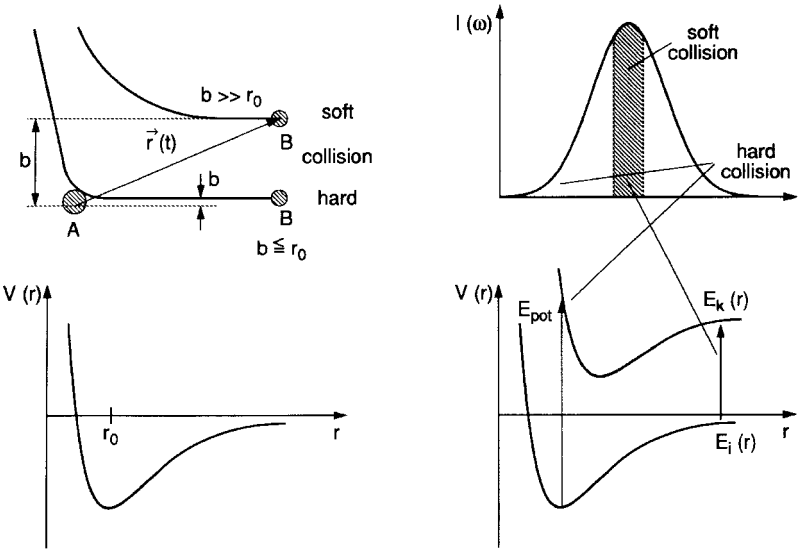

Fig. 8.1. Interaction potential $V(r)$ and semiclassical model for soft collisions with impact parameter $b \gg r_0$ and hard collisions ($b < r_0$)

interaction potential $V(\boldsymbol{r}, E_A, E_B)$, which may depend on the internal energies E_A and E_B of the collision partners. In most models a spherically symmetric potential $V(r)$ is assumed, which may have a minimum at $r = r_0$ (Fig. 8.1). If the impact parameter b is large compared to r_0 the collision is classified as a *soft* collision, while for $b \leq r_0$ *hard* collisions occur.

For soft collisions B passes only through the long-range part of the potential and the scattering angle θ is small. The shift ΔE of the energy levels of A or B during the collision is accordingly small. If one of the collision partners absorbs or emits radiation during a soft collision, its frequency distribution will be only slightly changed by the interaction between A and B. Soft collisions therefore contribute to the kernel of a collision-broadened line, that is, the spectral range around the line center.

For *hard* collisions, on the other hand, the collision partners pass through the short-range part of their interaction potential, and the level shift ΔE during the collision is correspondingly larger. Hard collisions therefore contribute to the line wings (Fig. 3.1).

8.1.1 Sub-Doppler Spectroscopy of Collision Processes

In Doppler-limited spectroscopy the effect of collisions on the line kernel is generally completely masked by the much larger Doppler width. Any information on the collision can therefore be extracted only from the line wings of the Voigt profile (Sect. 3.2), by a deconvolution of the Doppler-broadened Gaussian profile and the Lorentzian profile of collisional broadening [8.15]. Since the collisional linewidth increases proportionally to the pressure, reliable measurements are only possible at higher pressures where collisional broadening becomes comparable to the Doppler width. At such high pressures, however, many-body collisions may no longer be negligible, since the probability that N atoms are found simultaneously within a volume $V \approx r^3$ increases with the Nth power of the density. This implies that not only two-body collisions between A and B but also many-body collisions $A + N \cdot B$ may contribute to line profile and line shift of transitions in A. In such cases the line profile no longer yields unambiguous information on the interaction potential $V(A, B)$ [8.16].

With techniques of sub-Doppler spectroscopy, even small collisional broadening effects can be investigated with high accuracy. One example is the measurement of pressure broadening and shifts of narrow Lamb dips (Sect. 2.2) of atomic and molecular transitions, which is possible with an accuracy of a few kilohertz if stable lasers are used. The most accurate measurements have been performed with stabilized HeNe lasers on the transitions at 633 nm [8.17] and 3.39 μm [8.18]. When the laser frequency ω is tuned across the absorption profiles of the absorbing sample inside the laser resonator, the output power of the laser $P_L(\omega)$ exhibits sharp Lamb peaks (inverse Lamb dips) at the line centers of the absorbing transitions (Sect. 2.3). The line profiles of these peaks are determined by the pressure in the absorption cell, by saturation broadening, and by transit-time broadening (Sect. 3.4).

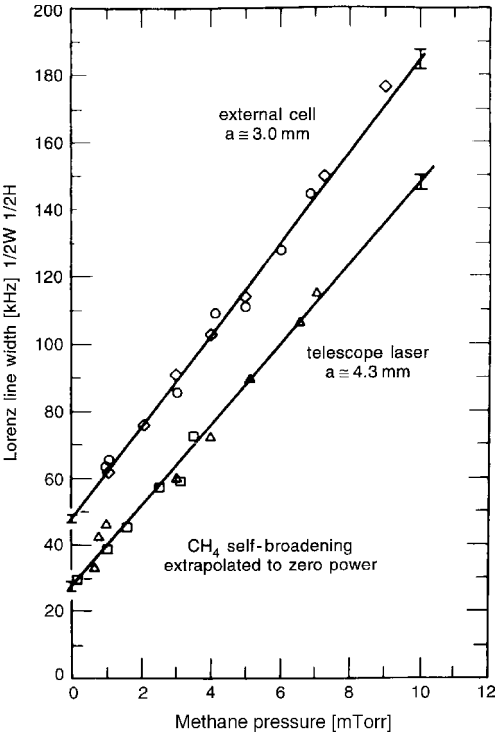

Fig. 8.2. Linewidth of the Lamb peak in the output power of a HeNe laser at $\lambda = 3.39\,\mu m$ with an intracavity CH_4 absorption cell and different beam waists of the expanded laser beam, causing a different transit-time broadening [8.18]

Center frequency ω_0, linewidth $\Delta\omega$, and line profile $P_L(\omega)$ are measured as a function of the pressure p (Fig. 8.2). The slope of the straight line $\Delta\omega(p)$ yields the line-broadening coefficient [8.19], while the measurement of $\omega_0(p)$ gives the collision-induced line shift.

A more detailed consideration of collisional broadening of Lamb dips or peaks must also take into account velocity-changing collisions. In Sect. 2.2 it was pointed out that only molecules with the velocity components $v_z = 0 \pm \gamma/k$ can contribute to the simultaneous absorption of the two counterpropagating waves. The velocity vectors $\boldsymbol{v}$ of these molecules are confined to a small cone within the angles $\beta \leq \pm\epsilon$ around the plane $v_z = 0$ (Fig. 8.3a), where

$$\sin\beta = v_z/|\boldsymbol{v}| \Rightarrow \sin\varepsilon \leq \gamma/(k \cdot v)\,, \text{ with } \quad v = |\boldsymbol{v}|\ . \tag{8.1}$$

During a collision a molecule is deflected by the angle $\theta = \beta'' - \beta$ (Fig. 8.3c). If $v \cdot \sin\theta < \gamma/k$, the molecule after the collision is still in resonance with the standing light wave inside the laser resonator. Such soft collisions with deflection angles $\theta < \epsilon$ therefore do not appreciably change the absorption probability of a molecule. Because of their statistical phase jumps (Sect. 3.3) they do, however, contribute to the linewidth. The line profile of the Lamb dip broadened by soft collisions remains Lorentzian.

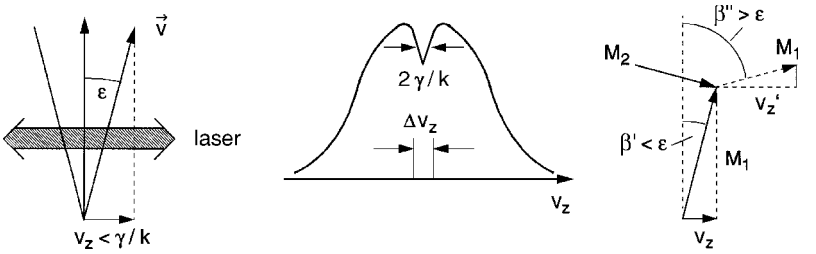

Fig. 8.3. Only molecules with velocity vectors within the angular range $\beta \leq \epsilon$ around the plane $z = 0$ contribute to the line profile of the Lamb dip. Velocity-changing collisions that increase β to values $\beta > \epsilon$ push the molecules out of resonance with the laser field

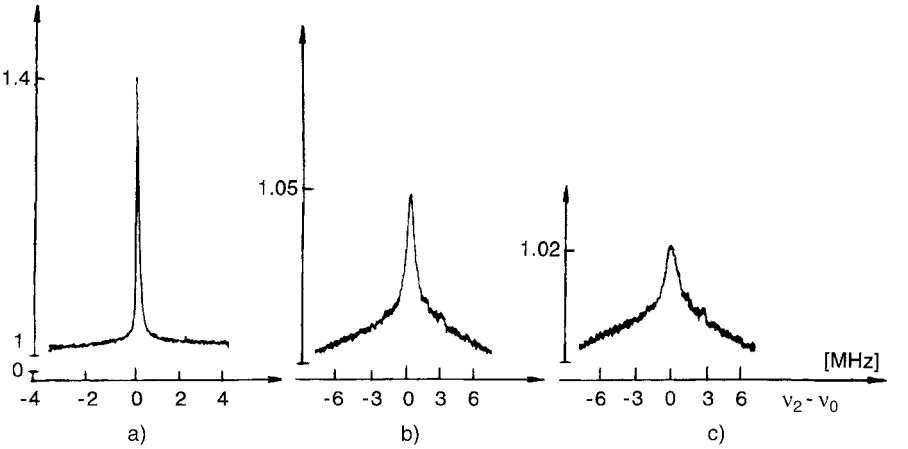

Fig. 8.4a–c. Line profiles of Lamb peaks of a HeNe laser at $\lambda = 3.39\,\mu m$ with intracavity CH_4 absorption cell: (**a**) pure CH_4 at 1.4 mbar; (**b**) addition of 30 mbar He; and (**c**) 79 mbar He [8.20]

Collisions with $\theta > \epsilon$ may shift the absorption frequency of the molecule out of resonance with the laser field. After a hard collision the molecule, therefore, can only contribute to the absorption in the line wings.

The combined effect of both kinds of collisions gives a line profile with a kernel that can be described by a Lorentzian profile slightly broadened by soft collisions. The wings, however, form a broad background caused by velocity-changing collisions. The whole profile cannot be described by a single Lorentzian function. In Fig. 8.4 such a line profile is shown for the Lamb peak in the laser output $P_L(\omega)$ at $\lambda = 3.39\,\mu m$ with a methane cell inside the laser resonator for different pressures of CH_4 and He [8.20].

8.1.2 Combination of Different Techniques

Often the collisional broadening of the Lamb dip and of the Doppler profile can be measured simultaneously. A comparison of both broadenings allows

the separate determination of the different contributions to line broadening. For phase-changing collisions there is no difference between the broadenings of the two different line profiles. However, velocity-changing collisions do affect the Lamb-dip profile (see above), but barely affect the Doppler profile because they mainly cause a redistribution of the velocities but do not change the temperature.

Since the homogeneous width γ of the Lamb-dip profile increases with pressure p, the maximum allowed deflection angle ϵ in (8.1) also increases with p. A comparison of pressure-induced effects on the kernel and on the background profile of the Lamb dips and on the Doppler profile therefore yields more detailed information on the collision processes. Velocity-selective optical pumping allows the measurement of the shape of velocity-changing collisional line kernels over the full thermal range of velocity changes [8.21].

Collisions may also change the orientation of atoms and molecules (Sect. 5.1), which means that the orientational quantum number M of an optically pumped molecule is altered. This can be monitored by polarization spectroscopy (Sect. 2.4). The orientation of molecules within the velocity interval $\Delta v_z = (\omega_p \pm \gamma)/k$ induced by the polarized pump radiation with frequency ω_p determines the polarization characteristics of the transmitted probe laser wave at frequency ω and therefore the detected signal $S(\omega)$. Any collision that alters the orientation, the population density N_i of molecules in the absorbing level $|i\rangle$, or the velocity v of absorbing molecules affects the line profile $S(\omega)$ of the polarization signal. The velocity-changing collisions have the same effect on $S(\omega)$ as on the Lamb-dip profiles in saturation spectroscopy. The orientation-changing collisions decrease the magnitude of the signal $S(\omega)$, while inelastic collisions result in the appearance of new *satellite polarization signals* in neighboring molecular transitions (Sect. 8.2). Orientation-changing collisions may also be detected with OODR saturation spectroscopy (Sect. 5.4) if the Lamb-dip profile is measured in dependence on the pressure for different angles α between the polarization planes of the linearly polarized pump and probe waves.

A commonly used technique for the investigation of depolarizing collisions in *excited* states is based on the orientation of atoms or molecules by optical pumping with a polarized laser and the measurement of the degree of polarization $P = (I_\parallel - I_\perp)/(I_\parallel + I_\perp)$ of the fluorescence emitted from the optically pumped or the collisionally populated levels (Sect. 8.2).

Because of the large mean radius $\langle r_n \rangle \propto n^2$ of the Rydberg electron, Rydberg atoms or molecules have very large collision cross sections. Therefore optical transitions to Rydberg states show large collisional broadening, which can be studied with Doppler-free two-photon spectroscopy or with two-step excitation (Sect. 5.4). For illustration, Fig. 8.5 illustrates pressure broadening and shifts of a rotational transition to a Rydberg level of the Li_2 molecule measured with Doppler-free OODR polarization spectroscopy (Sect. 5.5) in a lithium/argon heat pipe [8.22], where the intermediate level $B(v', J')$ was pumped optically by a circularly polarized pump laser. For the chosen temperature and pressure conditions the argon is confined to the cooled outer parts of the heat pipe, and the center of the heat pipe contains pure lithium

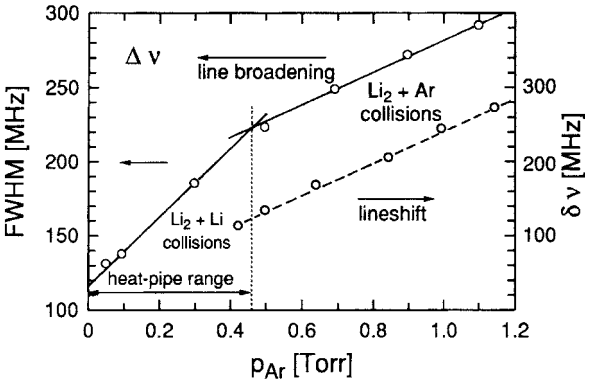

Fig. 8.5. Pressure broadening (*left scale*) and shift (*right scale*) of a Doppler-free rotational line in the Rydberg system $B\,^1\Sigma_u \rightarrow 6d\delta\,^1\Delta_g$ of the Li_2 molecule in a heat pipe for $Li_2^* + Li$ collisions at $p < 0.4$ mbar and for $Li_2^* + Ar$ collisions for $p > 0.4$ mbar [8.23]

vapor (98% Li atoms and 2% Li_2 molecules) with a total vapor pressure $p(L_i) = p(Ar)$ up to argon pressures of 0.7 mbar. The observed pressure broadening and shift in this range $p < 0.7$ mbar are therefore caused by $Li_2^* +$ Li collisions.

For $p(Ar) > 0.7$ mbar (0.5 torr) the argon begins to diffuse into the central part, if the temperature and thus the lithium vapor pressure remains constant while $p(Ar)$ increases. The slope of the curve $\Delta\omega(p)$ yields for $p >$ 0.7 mbar the cross section for $Li_2^* + Ar$ collisions. For the example depicted in Fig. 8.5 the cross sections for line broadening are $\sigma(Li_2^* + Li) = 60\,nm^2$ and $\sigma(Li_2^* + Ar) = 41\,nm^2$, whereas the line shifts are $\partial\nu/\partial p = -26$ MHz/mbar for $Li_2^* + Ar$ collisions [8.23]. Similar measurements have been performed on Sr Rydberg atoms [8.24], where the pressure shift and broadenings of Rydberg levels $R(n)$ for the principle quantum numbers n in the range $8 \leq n \leq 35$ were observed.

8.2 Measurements of Inelastic Collision Cross Sections of Excited Atoms and Molecules

Inelastic collisions transfer the internal energy of an atom or molecule A either into internal energy of the collision partner B or into relative kinetic energy of both partners. In the case of atoms, either *electronic* internal energy can be transferred to the collision partner or the magnetic energy of spin-orbit interaction. In the first case this leads to collision-induced transitions between different electronic states, and in the second case to transitions between atomic fine-structure components [8.24]. For *molecules* many more possibilities for energy transfer by inelastic collisions exist, such as rotational–vibrational or electronic energy transfer, and collision-induced dissociation.

A large variety of different spectroscopic techniques has been developed for the detailed investigation of these various inelastic collisions. They are illustrated in the following sections.

8.2.1 Measurements of Absolute Quenching Cross Sections

In Sect. 6.3 we saw that the effective lifetime $\tau_k^{\text{eff}}(N_B)$ of an excited level $|k\rangle$ of an atom or molecule A depends on the density N_B of the collision partners B. From the slope of the Stern–Volmer plot

$$1/\tau_k^{\text{eff}} = 1/\tau_k^{\text{rad}} + \sigma_k^{\text{total}} \overline{v} N_B \,, \tag{8.2}$$

the total deactivation cross section σ_k^{total} can be obtained, see (6.60). Since the collisional deactivation diminishes the fluorescence intensity emitted by $|k\rangle$, the inelastic collisions are called *quenching collisions* and σ_k^{total} is named the *quenching cross section*.

Several possible decay channels contribute to the depopulation of level $|k\rangle$, and the quenching cross section can be written as the sum

$$\sigma_k^{\text{total}} = \sum_m \sigma_{km} = \sigma_k^{\text{rot}} + \sigma_k^{\text{vib}} + \sigma_k^{\text{el}} \,, \tag{8.3}$$

over all collision-induced transitions $|k\rangle \rightarrow |m\rangle$ into other levels $|m\rangle$, which might be rotational, vibrational, or electronic transitions (Fig. 8.6).

While measurements of the effective lifetime $\tau_k^{\text{eff}}(N_B)$ yield *absolute* values of the *total quenching cross section* σ_k^{total}, the different contributions in (8.3) have to be determined by other techniques, such as LIF spectroscopy. Even if only their *relative* magnitudes can be measured, this is sufficient to obtain, together with the absolute value of σ^{total}, their absolute magnitudes.

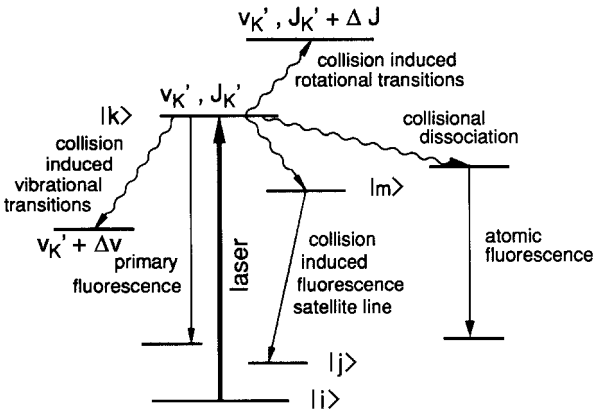

Fig. 8.6. Schematic term diagram for illustration of different possible inelastic collisional transitions of an optically pumped level $|k\rangle = (v'_k, J'_k)$ of a molecule M^*

8.2.2 Collision-Induced Rovibronic Transitions in Excited States

When the level $|k\rangle = |v', J'_k\rangle$ of an excited molecule M^* has been selectively populated by optical pumping, inelastic collisions $M^* + B$, which occur during the lifetime τ_k, will transfer $M^*(k)$ into other levels $|m\rangle = |v'_k + \Delta v, J'_k + \Delta J\rangle$ of the same or of another electronic state:

$$M^*(v'_k, J'_k) + B \rightarrow M^*(v'_k + \Delta v, J'_k + \Delta J) + B^* + \Delta E_{\text{kin}} \,. \tag{8.4}$$

The difference $\Delta E = E_k - E_m$ of the internal energies before and after the inelastic collision is transferred either into internal energy of B or into translation energy of the collisions partners.

Molecules in the collisionally populated levels $|m\rangle$ can decay by the emission of fluorescence or by further collisions. In the LIF spectrum new lines then appear besides the *parent lines*, which are emitted from the optically pumped level (Fig. 8.7). These new lines, called *collision-induced satellites* contain *the complete information on the collision process that has generated them.* Their wavelength λ allows the assignment of the upper level $|m\rangle = (v'_k + \Delta v, J'_k + \Delta J)$, their intensities yield the collisional cross sections σ_{km}, and their degree of polarization compared with that of the parent

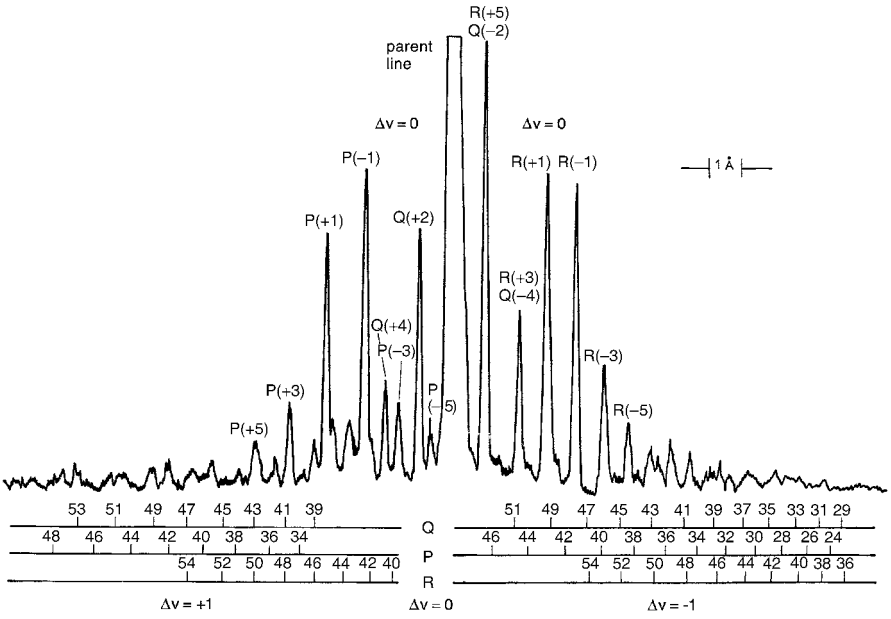

Fig. 8.7. Collision-induced satellite lines $Q(\Delta J')$, $R(\Delta J')$, and $P(\Delta J')$ in the LIF spectrum of Na_2 under excitation of the rotational level $B^1\Pi_u(v' = 6, J' = 43)$. The parent line is recorded with one-twentieth the sensitivity. The high satellite lines are related to $\Delta v = 0$ transitions and partly superimpose the weaker satellites from $\Delta v = \pm 1$ collision-induced transitions [8.29]

line gives the cross section for depolarizing, that is, orientation-changing collisions. This can be seen as follows:

Assume the upper level $|k\rangle$ is optically pumped on the transition $|i\rangle \rightarrow |k\rangle$ (Fig. 8.6) with a pump rate $N_i P_{ik}$ and collisions induce transitions $|k\rangle \rightarrow |m\rangle$. The rate equation for the population densities N_k, N_m can be written as

$$\frac{\mathrm{d}N_k}{\mathrm{d}t} = N_i P_{ik} - N_k \left(A_k + \sum_m R_{km} \right) + \sum_n N_n R_{nk} \,, \tag{8.5a}$$

$$\frac{\mathrm{d}N_m}{\mathrm{d}t} = N_k R_{km} - N_m \left(A_m + \sum_m R_{mn} \right) + \sum_n N_n R_{nm} \,, \tag{8.5b}$$

where the last two terms describe the collisional depopulation $|m\rangle \rightarrow |n\rangle$ and the repopulation $|n\rangle \rightarrow |k\rangle$ or $|n\rangle \rightarrow |m\rangle$ from other levels $|n\rangle$.

Under stationary conditions (optical pumping with a cw laser) $(\mathrm{d}N_k/\mathrm{d}t) = (\mathrm{d}N_m/\mathrm{d}t) = 0$. If the thermal population N_n is small (that is, $E_n \gg kT$) the last terms in (8.5) demand at least two successive collisional transitions $|k\rangle \rightarrow |n\rangle \rightarrow |k\rangle$ or $|k\rangle \rightarrow |n\rangle \rightarrow |m\rangle$, respectively, during the lifetime τ, which means a high collision rate. At sufficiently low pressures they can therefore be neglected.

From (8.5) the stationary population densities N_k, N_m are then obtained as

$$N_k = \frac{N_i P_{ik}}{A_k + \sum R_{km}} \,,$$

$$N_m = \frac{N_k R_{km} + \sum N_n R_{nm}}{A_m + \sum R_{mn}} \simeq N_k \frac{R_{km}}{A_m} \,. \tag{8.6}$$

The ratio of the fluorescence intensities of satellite line $|m\rangle \rightarrow |j\rangle$ to parent line $|k\rangle \rightarrow |i\rangle$

$$\frac{I_{mj}}{I_{ki}} = \frac{N_m A_{mj} h\nu_{mj}}{N_k A_{ki} h\nu_{ki}} = R_{km} \frac{A_{mj}\nu_{mj}}{A_m A_{ki}\nu_{ki}} \,, \tag{8.7}$$

directly yields the probability R_{km} for collision-induced transitions $|k\rangle \rightarrow |m\rangle$, if the relative radiative transition probabilities A_{mj}/A_m and A_{ki}/A_k are known. Measurements of the spontaneous lifetime τ_k and τ_m (Sect. 6.3) allow the determination of $A_k = 1/\tau_k$ and $A_m = 1/\tau_m$. The absolute values of A_{mj} and A_{ki} can then be obtained by measuring the *relative* intensities of all fluorescence lines emitted by $|m\rangle$ and $|k\rangle$ under collision-free conditions.

The probability R_{km} is related to the collision cross section σ_{km} by

$$R_{km} = (N_\mathrm{B}/\overline{v}) \int \sigma_{km}(v_\mathrm{rel}) v_\mathrm{rel}\, \mathrm{d}v \,, \tag{8.8}$$

where N_B is the density of collision partners B, and v_{rel} the relative velocity between M and B.

When the experiments are performed in a cell at temperature T, the velocities follow a Maxwellian distribution, and (8.8) becomes

$$R_{km} = N_B \left(\frac{8kT}{\pi\mu}\right)^{-1/2} \langle\sigma_{km}\rangle \ , \tag{8.9}$$

where $\mu = m_M m_B/(m_M + m_B)$ is the reduced mass, and $\langle\sigma_{km}\rangle$ means the average of $\sigma_{km}(v)$ over the velocity distribution. The cross sections σ_{km} obtained in this way represent integral cross sections, integrated over all scattering angles θ.

Such determinations of rotationally inelastic integral cross sections σ_{km} for collision-induced transitions in excited molecules obtained from measurements of satellite lines in the fluorescence spectrum have been reported for a large variety of different molecules, such as I_2 [8.25, 8.26], Li_2 [8.27, 8.28], Na_2 [8.29], or NaK [8.30]. For illustration, the cross section $\sigma(\Delta J)$ for the transition $J \rightarrow J + \Delta J$ in excited Na_2^* molecules induced by collisions $Na_2^* + He$ are plotted in Fig. 8.8. They rapidly decrease from a value $\sigma(\Delta J = \pm 1) \approx 0.3\,nm^2$ to $\sigma(\Delta J = \pm 8) \approx 0.02\,nm^2$. This decrease is essentially due to energy and momentum conservation, since the energy difference $\Delta E = E(J \pm \Delta J) - E(J)$ has to be transferred into the kinetic energy of the collision partners. The probability for this energy transfer is proportional to the Boltzmann factor $\exp[-\Delta E/(kT)]$ [8.31].

For interaction potentials $V(R)$ of the collision pair M + B with spherical symmetry, which only depend on the internuclear distance R, no internal angular momentum of M can be transferred. The absolute values of the cross sections $\sigma(\Delta J)$ are therefore a measure for the *nonspherical* part of the

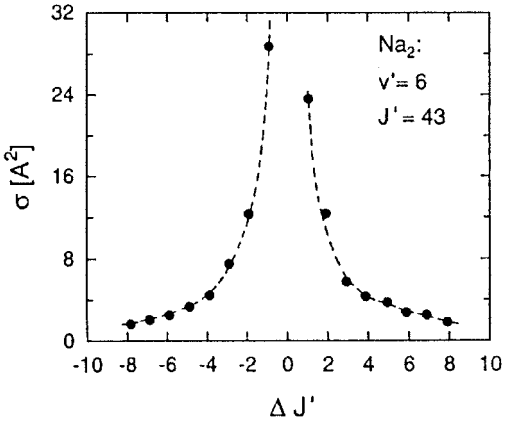

Fig. 8.8. Absolute integral cross sections $\sigma(\Delta J')$ for collision-induced rotational transitions when $Na_2^*(B\,^1\Pi_u, v' = 6, J' = 43)$ collides with He-atoms at $T = 500\,K$ [8.29]

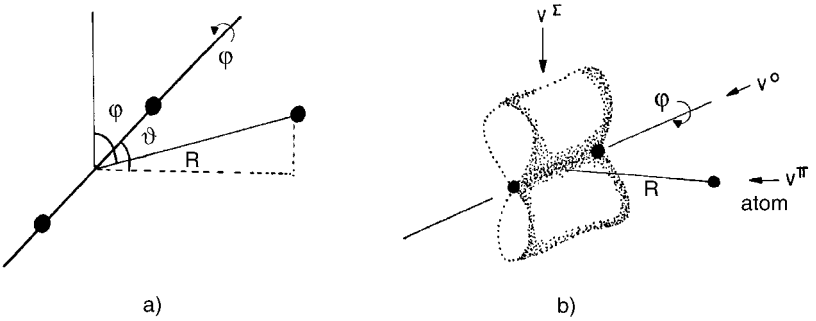

Fig. 8.9. (**a**) Illustration of the variables R, θ, and φ in the interaction potential $V(R, \theta, \varphi)$. (**b**) Schematic electron cloud distribution for excited homonuclear diatomic molecules in a Π state. Also shown are the two directions of φ for a Σ-type and a Π-type interaction potential

potential V(M, B). This potential can be represented by the expansion

$$V(R, \theta, \phi) = V_0(R) + \sum_{\ell,m} a_{\ell m} Y_\ell^m(\phi) \,, \tag{8.10}$$

where the Y_ℓ^m denote the spherical surface functions. A homonuclear diatomic molecule M in a Σ state has a cylindrically symmetric electron cloud. Its interaction potential must be independent of ϕ and furthermore has a symmetry plane perpendicular to the internuclear axis. For such symmetric states (8.10) reduces to

$$V(R, \theta) = a_0 V_0(R) + a_2 P_2(\cos\theta) + \ldots \,, \tag{8.11}$$

where the coefficient a_2 of the Legendre polynomical $P_2(\cos\theta)$ can be determined from $\sigma(\Delta J)$, while a_0 is related to the value of the elastic cross section [8.32, 8.33].

In a Π state, however, the electron cloud possesses an electronic angular momentum and the charge distribution no longer has cylindrical symmetry (Fig. 8.9b). The interaction potential $V(R, \theta, \phi)$ depends on all three variables. Since the two Λ components of a rotational level in a Π state ($\Lambda = 1$) correspond to different charge distributions, different magnitudes of the cross sections $\sigma(J, \pm\Delta J)$ for collision-induced rotational transitions are expected for the two Λ components of the same rotational level $|J\rangle$ [8.34, 8.35]. Such an asymmetry, which can be recognized in Fig. 8.7 (transitions with $\Delta J =$ even reach other Λ components than those with $\Delta J =$ odd), has indeed been observed [8.28, 8.34, 8.36].

In addition to LIF resonant two-photon ionization (Sect. 1.4) can also be used for the sensitive detection of collision-induced rotational transitions. This method represents an efficient alternative to LIF for those electronic states that do not emit detectable fluorescence because there are no allowed optical transitions into lower states. An illustrative example is the detailed

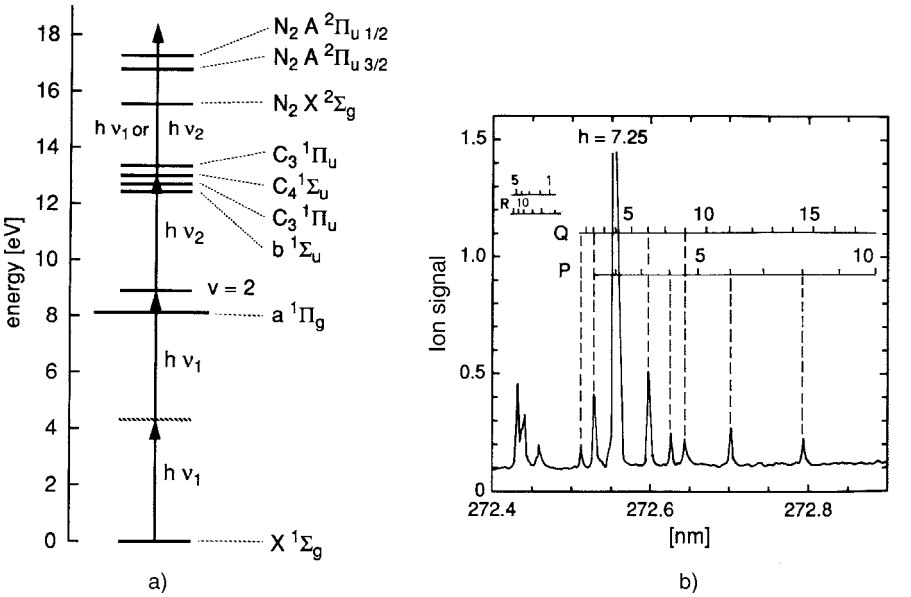

Fig. 8.10a,b. Term diagram for selective excitation of the level ($v' = 2$, $J' = 7$) in the $a^1\Pi_g$ state of N_2 with the detection of collisional transitions by resonant two-photon ionization [8.37]

investigation of inelastic collisions between excited N_2 molecules and different collision partners [8.37]. A vibration–rotation level (v', J') in the a $^1\Pi_g$ state of N_2 is selectively populated by two-photon absorption (Fig. 8.10). The collision-induced transitions to other levels ($v' + \Delta v$, $j' + \Delta J$) are monitored by resonant two-photon ionization (REMPI, Sect. 1.2) with a pulsed dye laser. The achievable good signal-to-noise ratio is demonstrated by the collisional satellite spectrum in Fig. 8.10b, where the optically pumped level was ($v' = 2$, $J' = 7$). This level is ionized by the $P(7)$ *parent line* in the spectrum, which has the signal height 7.25 on the scale of Fig. 8.10b.

If the parent level $|k\rangle = (v_k, J_k)$ of the optically pumped molecule has been oriented by polarized light, this orientation is partly transferred by collisions to the levels ($v_k + \Delta v$, $J_k + \Delta J$). This can be monitored by measuring the polarization ratio $R_p = (I_\parallel - I_\perp)/(I_\parallel + I_\perp)$ of the collisional satellite lines in the fluorescence [8.38].

The cross sections for collision-induced vibrational transitions are generally much smaller than those for rotational transitions. This is due to energy conservation (if $\Delta E_{vib} \gg kT$) and also to dynamical reasons (the collision has to be sufficiently nonadiabatic, that is, the collision time should be comparable or shorter than the vibrational period) [8.33]. The spectroscopic detection is completely analogous to that for rotational transitions. In the LIF spectrum new collision-induced bands $(v_k + \Delta_k) \rightarrow (v_m)$ appear (Fig. 8.7), with a rotational distribution that reflects the probabilities of collision-induced transitions $(v_k, J_k) \rightarrow (v_k + \Delta_v, J_k + \Delta J)$ [8.27, 8.29, 8.39, 8.40].

Vibrational transitions within the electronic ground state can be studied by time-resolved infrared spectroscopy or by pump–probe measurements (Sect. 8.3.1).

8.2.3 Collisional Transfer of Electronic Energy

Collisions may also transfer electronic energy. For instance, the electronic energy of an excited atom A^* or molecule M^* can be converted in a collision with a partner B into translational energy E_{kin} or, with higher probability, into internal energy of B [8.8].

For collisions at thermal energies the collision time $T_{coll} = d/\overline{v}$ is long compared to the time for an electronic transition. The interaction $V(A^*, B)$ or $V(M^*, B)$ can then be described by a potential. Assume that the two potential curves $V(A_i, B)$ and $V(A_k, B)$ cross at the energy $E(R_c)$ (Fig. 8.11). If the relative kinetic energy of the collision partners is sufficiently high to reach the crossing point, the collision pair may jump over to the other potential curve [8.41]. In Fig. 8.11, for instance, a collision $A_i + B$ can lead to electronic excitation $|i\rangle \rightarrow |k\rangle$ if $E_{kin} > E_2$, while for a collisional deexcitation $|k\rangle \rightarrow |i\rangle$ only the kinetic energy $E_{kin} > E_1$ is required.

The cross sections of electronic energy transfer $A^* + B \rightarrow A + B^* + \Delta E_{kin}$ are particularly large in cases of energy resonance, which means $\Delta E(A^* - A) \simeq \Delta E(B^* - B) \rightarrow \Delta E_{kin} \leq kT$. A well-known example is the collisional excitation of Ne atoms by metastable He^* atoms, which represents the main excitation mechanism in the HeNe laser.

The experimental proof for such electronic energy transfer ($E \rightarrow E$ transfer) is based on the selective excitation of A by a laser and the spectrally resolved detection of the fluorescence from B^* [8.42, 8.43].

In collisions between excited atoms and molecules either the atom A^* or the molecule M^* may be electronically excited. Although the two cases

$$M(v_i'', J_i'') + A^* \rightarrow M^*(v', J') + A\,, \tag{8.12a}$$

and

$$M^*(v_k', J_k') + A \rightarrow M(v'', J'') + A^*\,, \tag{8.12b}$$

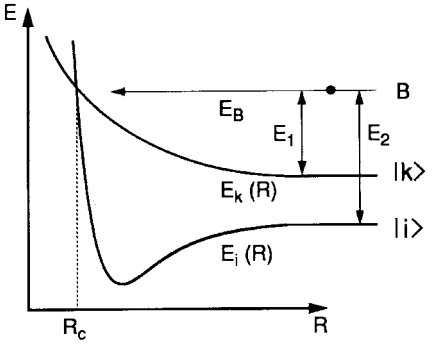

Fig. 8.11. Potential diagram for collision-induced transitions between the two electronic states $|i\rangle$ and $|k\rangle$ that can occur at the crossing point at $R = R_c$ of the two potential curves $E_i R = M_i + B$ and $E_k R = M_k + B$

represent inverse processes, their collision cross sections may differ considerably. This was demonstrated by the example M= Na_2, A= Na. Either the Na atoms were selectively excited into the 3P state and the fluorescence of Na_2^* was measured with spectral and time resolutions [8.44], or Na_2 was excited into a definite level (v_k', J_k') in the $^1A\Sigma_u$ state and the energy transfer was monitored by time-resolved measurements of the shortened lifetime $\tau_k(v_k', J_k')$ and the population $N_{3p}(t)$ of the Na* $(3P)$ level detected through the atomic fluorescence [8.45]. There are two distinct processes that lead to the formation of Na*:

(a) direct energy transfer according to (8.12b), or
(b) collision-induced dissociation $Na_2^* + Na \rightarrow Na^* + Na + Na$.

This collision-induced dissociation of electronically excited molecules plays an important role in chemical reactions and has therefore been studied for many molecules [8.46–8.48]. The collision cross sections for this process may be sufficiently large to generate inversion between atomic levels. Laser action based on *dissociation pumping* has been demonstrated. Examples are the powerful iodine laser [8.49] and the Cs laser [8.50].

The transfer of electronic energy into rovibronic energy has much larger cross sections than the electronic to translational energy $(E \rightarrow T)$ transfer [8.51]. These processes are of crucial importance in photochemical reactions of larger molecules and detailed studies with time-resolved laser spectroscopy have brought much more insight into many biochemical processes [8.52–8.54].

One example of a state-selective experimental technique well suited for studies of electronic to vibrational $(E \rightarrow V)$ transfer processes is based on CARS (Sect. 4.4). This has been demonstrated by Hering et al. [8.55], who studied the reactions

$$Na^*(3P) + H_2(v'' = 0) \rightarrow Na(3S) + H_2(v'' = 1, 2, 3)\,, \tag{8.13}$$

where Na* was excited by a dye laser and the internal state distribution of $H_2(v'', J'')$ was measured with CARS.

An interesting phenomenon based on collisions between excited atoms and ground-state atoms is the macroscopic diffusion of optically pumped atoms realized in the *optical piston* [8.56]. It is caused by the difference in cross sections for velocity-changing collisions involving excited atoms A* or ground-state atoms A, respectively, and results in a spatial separation between optically pumped and unpumped atoms, which can be therefore used for isotope separation [8.57].

8.2.4 Energy Pooling in Collisions Between Excited Atoms

Optical pumping with lasers may bring an appreciable fraction of all atoms within the volume of a laser beam passing through a vapor cell into an excited electronic state. This allows the observation of collisions between two *excited* atoms, which lead to many possible excitation channels where the

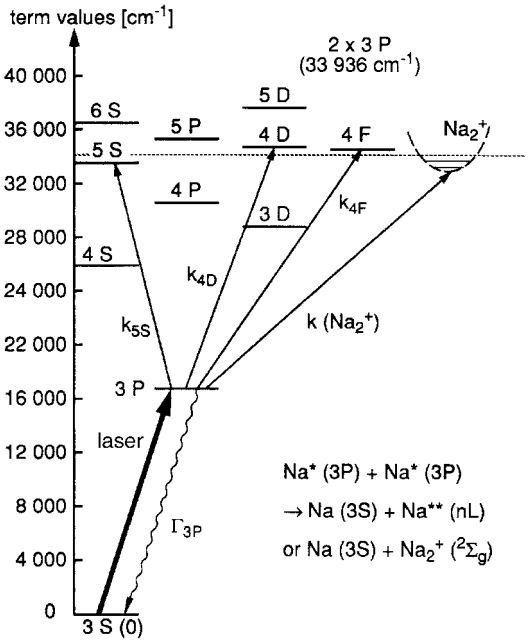

Fig. 8.12. Level diagram of the Na atom with schematic illustration of the different excitation channels in collisions $Na^*(3P) + Na^*(3P)$ [8.60]

sum of the excitation energies is accumulated in one of the collision partners. Such *energy-pooling* processes have been demonstrated for $Na^* + Na^*$, where reactions

$$Na^*(3P) + Na^*(3P) \rightarrow Na^{**}(nL) + Na(3S)\,, \tag{8.14}$$

have been observed [8.58], leading to the excitation of high-lying levels $|n, L\rangle$ (Fig. 8.12).

Measurements of the fluorescence intensity $I_{Fl}(n, L)$ emitted by the levels Na^{**} ($n, L = 4D$ or $5S$) yields the collision rate

$$k_{n,L} = N^2(Na^*3p) \cdot \sigma_{n,L}\overline{v} \quad [1/s\,cm^3]\,,$$

of optically pumped Na atoms, which increases with the square N^2 of the density of excited Na^* atoms. This density cannot be determined directly from the measured $Na^*(3P)$ fluorescence because radiation trapping falsifies the results [8.59]. The attenuation of the transmitted laser beam is a better measure because every absorbed photon produces one excited $Na^*(3P)$ atom.

Since the sum of the excitation energies of the two colliding $Na^*(3P)$ atoms is higher than the ionization limit of the Na_2 molecule, associative ionization

$$Na^*(3P) + Na^*(3P) \underset{k_{Na_2^+}}{\rightarrow} Na_2^+ + e^-\,, \tag{8.15}$$

can be observed. The measurement of Na_2^+ ions gives the reaction rate $k(Na_2^+)$ for this process [8.60].

A further experimental step that widens the application range is the excitation of two different species A_1 and A_2 with two dye lasers. An example is the simultaneous excitation of Na*(3P) and K*(4P) in a cell containing a mixture of sodium and potassium vapors. Energy pooling can lead to the excitation of high-lying Na** or K** states, which can be monitored by their fluorescence [8.61]. When both lasers are chopped at two different frequencies f_1 and f_2 (where $1/f$ is long compared to the collisional transfer time), lock-in detection of the fluorescence emitted from the highly excited levels at f_1, f_2 or $f_1 + f_2$ allows the distinction between the energy pooling processes $Na^* + Na^*$, $K^* + K^*$, and $Na^* + K^*$ leading to the excitation of the levels $|n, L\rangle$ of Na** or K**. For further examples see [8.62, 8.63].

8.2.5 Spectroscopy of Spin-Flip Transitions

Collision-induced transitions between fine-structure components where the relative orientation of the electron spin with respect to the orbital angular momentum is changed have been studied in detail by laser-spectroscopic techniques [8.64]. One of the methods often used is *sensitized fluorescence*, where one of the fine-structure components is selectively excited and the fluorescence of the other component is observed as a function of pressure [8.65]. Either pulsed excitation and time-resolved detection is used [8.66] or the intensity ratio of the two fine-structure components is measured under cw excitation [8.67].

Of particular interest is the question into which of the fine-structure components of the atoms a diatomic molecule dissociates after excitation into predissociating states. The investigation of this question gives information on the recoupling of angular momenta in molecules at large intermolecular distances and about crossings of potential curves [8.68]. Early measurements of these processes in cells often gave wrong answers because collision-induced fine-structure transitions and also radiation trapping had changed the original fine-structure population generated by the dissociation process. Therefore, laser excitation in molecular beams has to be used to measure the initial population of a certain fine-structure component [8.69].

Collision-induced spin-flip transitions in molecules transfer the optically excited molecule from a singlet into a triplet state, which may drastically change its chemical reactivity [8.70]. Such processes are important in dye lasers and have therefore been intensively studied [8.71]. Because of the long lifetime of the lowest triplet state T_0, its population $N(t)$ can be determined by time-resolved measurements of the absorption of a dye laser tuned to the transition $T_0 \rightarrow T_1$.

A laser-spectroscopic technique for investigations of spin-flip transitions under electron impact excitation of Na atoms [8.72] is shown in Fig. 8.13. Optical pumping with σ^+ light on the $3S_{1/2} \rightarrow 3P_{1/2}$ transition in an external weak magnetic field orients the Na atoms into the $3S_{1/2}(m_s = +1/2)$ level.

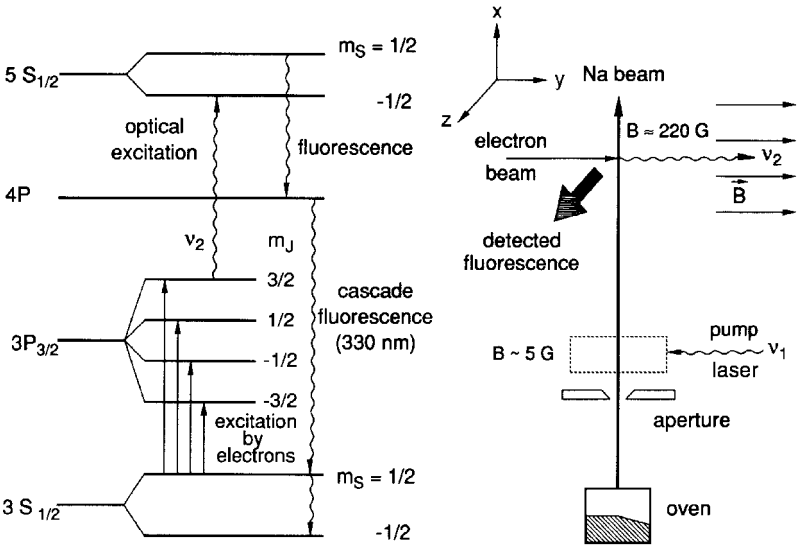

Fig. 8.13. The relative populations of Zeeman levels $|M_j\rangle$ in the $3\,^2P_{3/2}$ state of Na are probed by laser excitation of the $5\,^2S_{1/2}$ state, which is monitored via the cascade fluorescence into the $3\,S_{1/2}$ state [8.72]

Starting from this level the Zeeman components $3P_{3/2}(M_J)$ are populated by electron impact. The population N_M is probed by a cw dye laser tuned to the transitions $3^2P_{3/2}(M_J) \rightarrow 5^2S_{1/2}(M_s = \pm 1/2)$, which can be monitored by the cascade fluorescence $5S_{1/2} \rightarrow 4P \rightarrow 3S_{1/2}$.

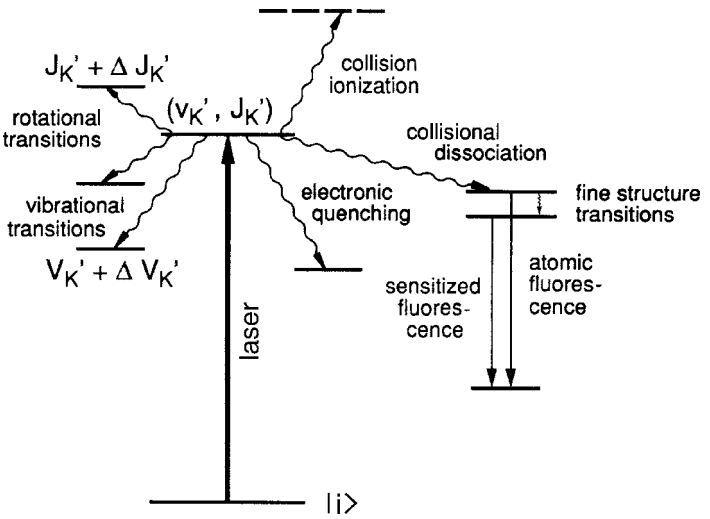

Fig. 8.14. Schematic diagram of all possible collision-induced transitions from a molecular level (v'_k, J'_k) in an excited electronic state selectively populated by optical pumping

Figure 8.14 summarizes all possible collision-induced transitions from a selectively excited molecular level $|v'_k, J'_k\rangle$ to other molecular or atomic levels.

8.3 Spectroscopic Techniques for Measuring Collision-Induced Transitions in the Electronic Ground State of Molecules

In the electronic ground states of molecules collision-induced transitions represent, for most experimental situations, the dominant mechanism for the redistribution of energy, because the radiative processes are generally too slow. In cases where a nonequilibrium distribution has been produced (for example, by chemical reactions or by optical pumping), these collisions try to restore thermal equilibrium. The relaxation time of the system is determined by the absolute values of collision cross sections.

For most infrared molecular lasers, such as the CO_2 and the CO laser, or for *chemical lasers*, such as the HF or HCl lasers, collisional energy transfer between vibrational–rotational levels of the lasing molecules plays a crucial role for the generation and maintenance of inversion and gain. These lasers are therefore called *energy-transfer lasers* [8.73]. Also in many visible molecular lasers, which oscillate on transitions between optically pumped levels (v', J') of the excited electronic state and high vibrational levels of the electronic ground state, collisional deactivation of the lower laser level is essential because the radiative decay is generally too slow. Examples are dye lasers [8.74] or dimer lasers, such as the Na_2 laser or the I_2 laser [8.75].

The internal energy $E_i = E_{\text{vib}} + E_{\text{rot}}$ of a molecule $M(v_i, J_i)$ in its electronic ground state may be transferred during a collision with another molecule AB

$$M(E_i) + AB(E_m) \rightarrow M(E_i - \Delta E_1) + AB^*(E_m + \Delta E_2) + \Delta E_{\text{kin}} , \qquad (8.16)$$

into vibrational energy of AB^* ($V \rightarrow V$ transfer), rotational energy ($V \rightarrow R$ transfer), electronic energy ($V \rightarrow E$ transfer), or translational energy ($V \rightarrow T$ transfer). In collisions of M with an atom A only the last two processes are possible.

The experiments show that the cross sections are much larger for $V \rightarrow V$ or $V \rightarrow R$ transfer than for $V \rightarrow T$ transfer. This is particularly true when the vibrational energies of the two collision partners are near resonant.

A well-known example of such a near-resonant $V \rightarrow V$ transfer is the collisional excitation of CO_2 molecules by N_2 molecules

$$CO_2(0, 0, 0) + N_2(v = 1) \rightarrow CO_2(0, 0, 1) + N_2(v = 0) , \qquad (8.17)$$

which represents the main excitation mechanism of the upper laser level in the CO_2 laser (Fig. 8.15) [8.76].

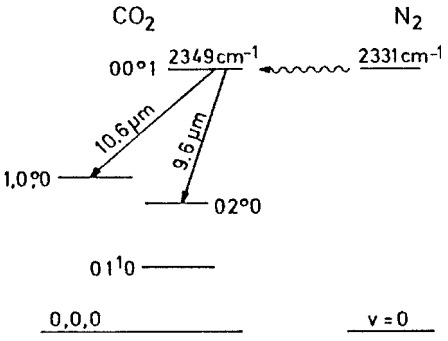

Fig. 8.15. Vibrational energy transfer from N_2 ($v = 1$) to the upper vibrational level ($v_1 = 0, v_2 = 0, l_{vib} = 0, v_3 = 1$) of the CO_2 laser transitions

The experimental techniques for the investigation of inelastic collisions involving molecules in their electronic ground state generally differ from those discussed in Sect. 8.2. The reasons are the long spontaneous lifetimes of ground-state levels and the lower detection sensitivity for infrared radiation compared to those for the visible or UV spectrum. Although infrared fluorescence detection has been used, most of the methods are based on absorption measurements and double-resonance techniques.

8.3.1 Time-Resolved Infrared Fluorescence Detection

The energy transfer described by (8.16) can be monitored if M^* is excited by a short infrared laser pulse and the fluorescence of AB^* is detected by a fast cooled infrared detector (Sect. 4.5) with sufficient time resolution. Such measurements have been performed in many laboratories [8.6]. For illustration, an experiment carried out by Green and Hancock [8.77] is explained by Fig. 8.16a: a pulsed HF laser excites hydrogen fluoride molecules into the vibrational level $v = 1$. Collisions with other molecules AB (AB = CO, N_2)

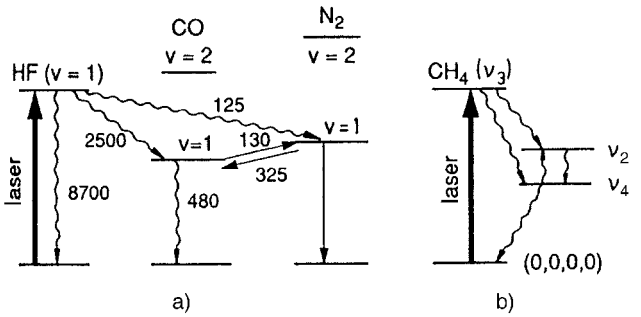

Fig. 8.16a,b. Fluorescence detection of vibrational energy transfer from an optically pumped molecular level: (**a**) intermolecular transfer $HF^* \rightarrow CO, N_2$. The mean numbers of collisions are given for the different collision-induced transitions. (**b**) *Intra*molecular transfer $CH_4^*(\nu_3) \rightarrow CH_4^*(\nu_2) + \Delta E_{kin}$ [8.77]

transfer the energy to excited vibrational levels of AB*. The infrared fluorescence emitted by AB* and HF* has to be separated by spectral filters. If two detectors are used, the decrease of the density $N(\mathrm{HF}^*)$ of vibrationally excited HF molecules and the build-up and decay of $N(\mathrm{AB}^*)$ can be monitored simultaneously.

For larger molecules M two different collisional relaxation processes have to be distinguished: collisions $\mathrm{M}^* + \mathrm{AB}$ may transfer the internal energy of M* to AB* (*inter*molecular energy transfer), or may redistribute the energy among the different vibrational modes of M* (*intra*molecular transfer) (Fig. 8.16b). One example is the molecule $\mathrm{M} = \mathrm{C_2H_4O}$, which can be excited on the C–H stretching vibration by a pulsed parametric oscillator at $3000\,\mathrm{cm}^{-1}$ [8.78]. The fluorescence emitted from other vibrational levels which are populated by collision-induced transitions is detected through spectral filters. Further examples can be found in several reviews [8.79–8.81].

8.3.2 Time-Resolved Absorption and Double-Resonance Methods

While collision-induced transitions in excited electronic states can be monitored through the satellite lines in the *fluorescence* spectrum (Sect. 8.2.2), inelastic collisional transfer in electronic ground states of molecules can be studied by changes in the *absorption* spectrum. This technique is particularly advantageous if the radiative lifetimes of the investigated rotational–vibrational levels are so long that fluorescence detection fails because of intensity problems.

A successful technique for studying collision-induced transitions in electronic ground states is based on time-resolved double resonance [8.82]. The method is explained by Fig. 8.17. A pulsed laser L1 tuned to an infrared or optical transition $|i\rangle \rightarrow |k\rangle$ depletes the lower level $|1\rangle = (v_i'', J_i'')$. The depleted level is refilled by collisional transitions from other levels. A second weak probe laser L2 is tuned to another transition $|1\rangle \rightarrow |3\rangle = (v_j', J_j')$ starting from the depleted lower level $|i\rangle$. If the pump and probe laser beams overlap within a path length Δz in the absorbing sample, the absorption of the probe laser radiation can be measured by monitoring the transmitted probe laser intensity

$$I(\Delta z, t) = I_0\,\mathrm{e}^{-\alpha \Delta z} \approx I_0[1 - N_i(t)\sigma_{ij}^{\mathrm{abs}}\Delta z]\,. \tag{8.18}$$

The time-resolved measurement of $I(\Delta z, t)$ yields the time dependence of the population density $N_i(t)$. Using a cw probe laser the absorption can be measured by the transmitted intensity $I(\Delta z, t)$, or by the time-dependent fluorescence induced by the probe laser, which is proportional to $N_j(t) \propto N_i(t) \cdot P(L_2)$. If a pulsed probe laser is used, the time delay Δt between pump and probe is varied and the measured values of $\alpha(\Delta t)$ yield the refilling time of level $|1\rangle$.

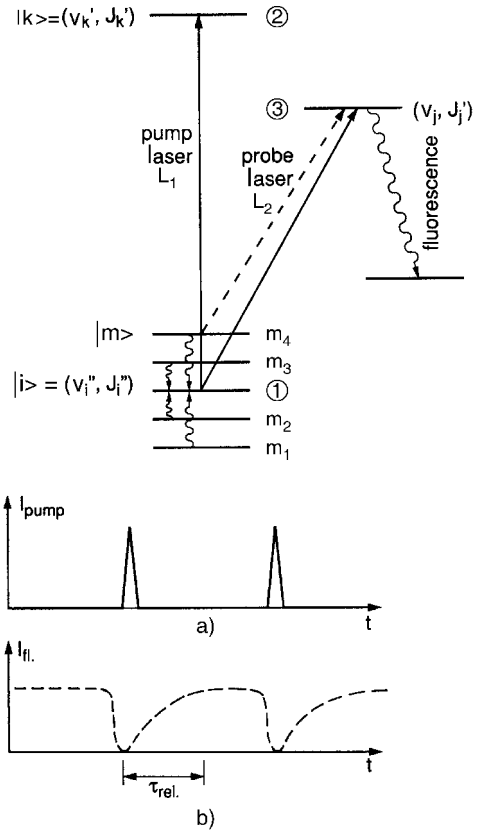

Fig. 8.17. (**a**) Level diagram for the determination of the refilling rate of a lower level (v_i'', J_i'') depleted by a pump laser pulse via measurements of the time-dependent probe laser absorption; (**b**) time dependence of pump pulses and level population $N_i(t)$ monitored via the probe laser-induced fluorescence

Without optical pumping the population densities are time independent at thermal equilibrium. From the rate equation

$$\frac{\mathrm{d}N_i^0}{\mathrm{d}t} = 0 = -N_i^0 \sum_m R_{im} + \sum_m N_m^0 R_{mi} \,, \tag{8.19}$$

we obtain the condition of *detailed balance*

$$N_i^0 \sum_m R_{im} = \sum_m N_m^0 R_{mi} \,, \tag{8.20}$$

where R_{im} are the relaxation probabilities for transitions $|i\rangle \rightarrow |m\rangle$. If the population N_i^0 is depleted to the saturated value $N_i^s < N_i^0$ by optical pumping at $t = 0$, the right side of (8.20) becomes larger than the left side and collision-induced transitions $|m\rangle \rightarrow |i\rangle$ from neighboring levels $|m\rangle$ refill $N_i(t)$. The time dependence $N_i(t)$ after the end of the pump pulse is obtained from

$$\frac{\mathrm{d}N_i}{\mathrm{d}t} = \sum_m N_m R_{mi} - N_i(t) \sum_m R_{im} \,. \tag{8.21a}$$

If we assume that optical pumping of level $|i\rangle$ does not essentially affect the population densities N_m $(m \neq i)$, we obtain from (8.20), (8.21a)

$$\frac{\mathrm{d}N_i}{\mathrm{d}t} = [N_i^0 - N_i(t)] \sum_m R_{im} = \left[N_i^0 - N_i(t)\right] K_i \,, \tag{8.21b}$$

with the relaxation rate

$$K_i = \sum_m R_{im} = N_\mathrm{B} \overline{v} \sigma_i^\mathrm{total} = N_\mathrm{B} \sqrt{\frac{8kT}{\pi\mu}} \left\langle \sigma_i^\mathrm{total} \right\rangle \,, \tag{8.22}$$

where N_B is the density of collision partners, $\mu = M_\mathrm{A} \cdot M_\mathrm{B}/(M_\mathrm{A} + M_\mathrm{B})$ the reduced mass and $\sigma_i^\mathrm{total} = \sum_m \sigma_{im}$ the total collision cross section.

The relaxation constant K_i depends on the total cross section $\langle \sigma_i^\mathrm{total} \rangle = \sum_m \langle \sigma_{im} \rangle$ averaged over the thermal velocity distribution and on the temperature T. Integration of (8.21) gives

$$N_i(t) = N_i^0 + \left[N_i^s(0) - N_i^0\right] \mathrm{e}^{-K_i t} \,. \tag{8.23}$$

This shows that after the end of the pump pulse at $t = 0$ the population density $N_i(t)$ returns exponentially from its saturated valued $N_i^s(0)$ back to its equilibrium value N_i^0 with the time constant

$$\tau = (K_i)^{-1} = \left(\overline{v}_\mathrm{rel} \left\langle \sigma_i^\mathrm{total} \right\rangle N_\mathrm{B}\right)^{-1} \,, \tag{8.24}$$

which depends on the averaged total refilling cross section $\langle \sigma_i^\mathrm{total} \rangle$ and on the number density N_B of collision partners.

One example of this pump-and-probe technique is the investigation of collision-induced vibrational–rotational transitions in the different isotopes HDCO and D_2CO of formaldehyde by an infrared–UV double resonance [8.83]. A CO_2 laser pumpes the ν_6 vibration of the molecule (Fig. 8.18). The collisional transfer into other vibrational modes is monitored by the fluorescence intensity induced by a tunable UV dye laser with variable time delay.

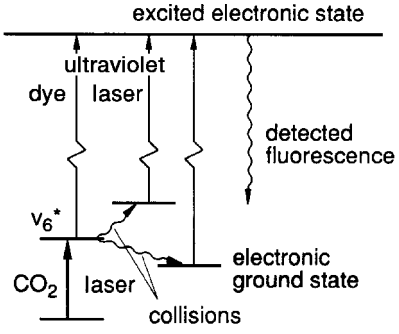

Fig. 8.18. Term diagram of IR–UV double resonance for measurements of collision-induced intramolecular vibrational transitions in the D_2CO molecule [8.83]

The time resolution of the pump-and-probe technique is not limited by the rise time of the detectors. It can therefore be used in the pico- and femtosecond range (Sect. 6.4) and is particularly advantageous for the investigation of ultrafast relaxation phenomena, such as collisional relaxation in liquids and solids [8.84, 8.85]. It is also useful for the detailed *real-time* study of the formation and dissociation of molecules where the collision partners are observed during the short time interval when forming or breaking a chemical bond [8.86].

8.3.3 Collision Spectroscopy with Continuous-Wave Lasers

State-selective measurements of the different contributions R_{im} in (8.3, 8.22) can be performed without time resolution if the absolute value of $\sigma_i^{\text{total}} = \sum \sigma_{im}$ is known from time resolved investigations, discussed in the previous section. The pump laser may be a cw dye laser that is tuned to the wanted transition $|i\rangle \rightarrow |k\rangle$ (Fig. 8.19) and is chopped at a frequency $f \ll 1/\tau_i = K_i$. This always guarantees quasi-stationary population densities N_i^s during the on phase and N_i^0 during the off phase of the pump laser.

In this case the deviation $N_i^s - N_i^0$ from thermal equilibrium during the on phase does affect via collisional transfer the population densities N_m of neighboring levels $|m\rangle$ (8.21a). Under stationary conditions we obtain in analogy to (8.19, 8.21) for the on-phase of the pump laser

$$\frac{\mathrm{d}N_m}{\mathrm{d}t} = 0 = \sum_j (N_j R_{jm} - N_m R_{mj}) - (N_m - N_m^0) K_m \,, \tag{8.25a}$$

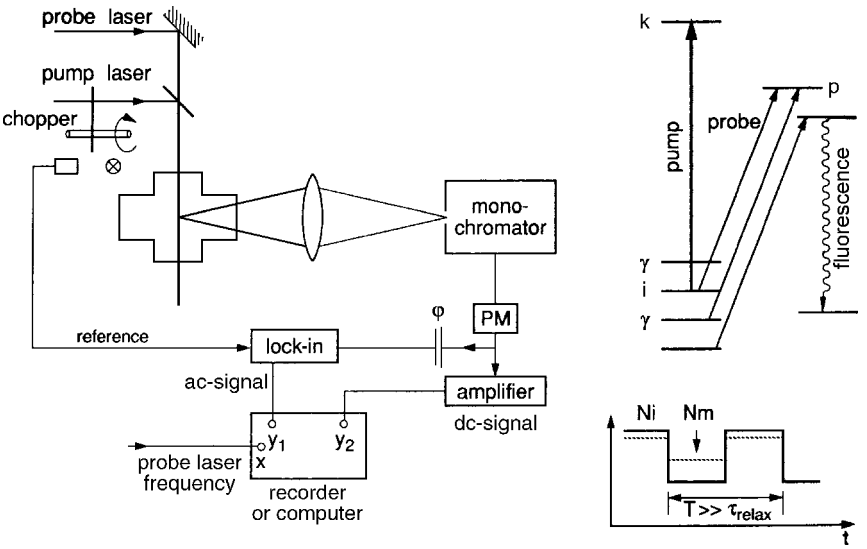

Fig. 8.19. Experimental arrangement and term diagram for measurements of individual collision-induced transitions in molecular electronic ground states with cw lasers

and for the off-phase

$$\frac{\mathrm{d}N_m^0}{\mathrm{d}t} = \sum_j N_j^0 R_{jm} - N_m^0 R_{mj} = 0 \,, \tag{8.25b}$$

where the right side of (8.25) represents the relaxation of N_m toward the equilibrium population N_m^0. Inserting the deviations $\Delta N = N - N^0$ into (8.25) yields with (8.19)

$$0 = \sum_j (\Delta N_j R_{jm} - \Delta N_m R_{mj}) - \Delta N_m K_m \;\Rightarrow\; \Delta N_m = \frac{\sum \Delta N_j R_{jm}}{\sum R_{mj} + K_m} \,. \tag{8.26}$$

This equation relates the population change ΔN_m with that of all other levels $|j\rangle$, where the sum over j also includes the optically pumped level $|i\rangle$. For $j \neq i$ the quantities ΔN_j and R_{jm} are proportional to the density N_B of the collision partners. At sufficiently low pressures we can neglect all terms $\Delta N_j \cdot R_{jm}$ for $j \neq i$ in (8.26) and obtain for the limiting case $p \to 0$ the relation

$$\frac{\Delta N_m}{\Delta N_i} = \frac{R_{im}}{\sum_j R_{mj} + K_m} \,. \tag{8.27}$$

The relaxation constant K_m can be obtained from a time-resolved measurement (Sect. 8.3.2). The signals from the chopped cw laser experiments give the following information: the ratio $\Delta N_m / \Delta N_i$ is directly related to the ratio of the ac absorption signals of the probe laser tuned to the transition $|i\rangle \to |p\rangle$ and $|m\rangle \to |p\rangle$, respectively, when the lock-in detector is tuned to the chopping frequency f of the pump laser. This means that the ratio

$$\frac{S_m^\mathrm{ac}}{S_i^\mathrm{ac}} = \frac{B_{mp} \Delta N_m}{B_{ip} \Delta N_i} \,, \tag{8.28}$$

of the ac signals is proportional to the ratio of the population changes and depends furthermore on the Einstein coefficients B_{mp} and B_{ip}.

If the time-averaged dc part of the probe laser signal

$$S_m^\mathrm{dc} = C B_{mp} \frac{(N_m^s + N_m^0}{2} \,, \tag{8.29}$$

for a square-wave modulation of the pump laser is also monitored, the relative changes $\Delta N_m / N_m$ of the population densities N_m can be obtained from the relations

$$\frac{\Delta N_m / N_m^0}{\Delta N_i / N_i^0} = \frac{S_m^\mathrm{ac}}{S_m^\mathrm{dc}} \frac{S_i^\mathrm{dc}}{S_i^\mathrm{ac}} \,. \tag{8.30}$$

With $N_i^0 / N_m^0 = (g_i / g_m) \exp(-\Delta E / kT)$, the absolute values of ΔN_m can be determined from (8.30).

8.3.4 Collisions Involving Molecules in High Vibrational States

Molecules in high vibrational levels $|v\rangle$ of the electronic ground state generally show much larger collision cross sections. If the kinetic energy E_{kin} of the collision partners exceeds the energy difference $(E_{\text{D}} - E_{\text{v}})$ between the dissociation energy E_{D} and the vibrational energy E_{v}, dissociation can take place (Fig. 8.20a). Since the resulting fragments often have a larger reactivity than the molecules, the probability for the initiation of chemical reactions generally increases with increasing vibrational energy. The investigation of collisions involving vibrationally excited molecules is therefore of fundamental interest. Several spectroscopic methods have been developed for achieving a sufficient population of high vibrational levels: optical pumping with infrared lasers with one- or multiple-photon absorption is a possibility for infrared-active vibrational transitions [8.87]. For homonuclear diatomics or for infrared-inactive modes, this method is not applicable.

Here, stimulated emission pumping is a powerful technique to achieve a large population in selected vibrational levels [8.88, 8.89]. While the pump laser is kept on the transition $|i\rangle \rightarrow |k\rangle$, the probe laser is tuned to the downward transition $|k\rangle \rightarrow |v\rangle$ (Fig. 8.20b). Proper selection of the upper level $|k\rangle$ allows one to reach sufficiently large Franck–Condon factors for the transition $|k\rangle \rightarrow |v\rangle$. With pulsed lasers a considerable fraction of the initial population N_i in the level $|i\rangle$ can be transferred into the final level $|v\rangle$.

With a coherent stimulated Raman process (STIRAP) (see Sect. 7.3), nearly the whole initial population N_i may be transferred into the final level $|v\rangle$ [8.90]. Here no exact resonance with the intermediate excited level $|k\rangle$ is wanted in order to avoid transfer losses by spontaneous emission from level $|k\rangle$. The population transfer can be explained by an adiabatic passage between *dressed states* (that is, states of the molecule plus the radiation field) [8.91, 8.92].

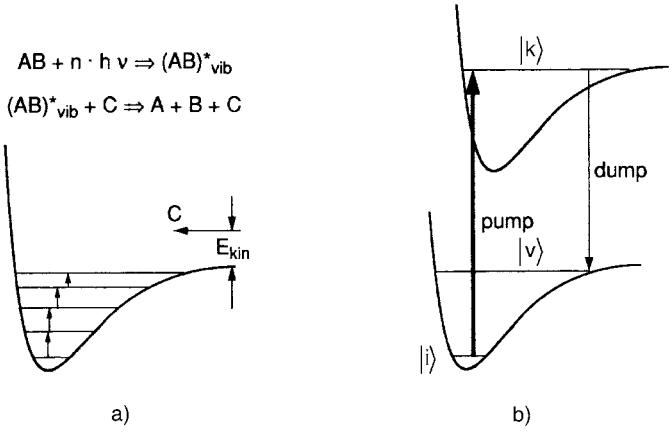

Fig. 8.20a,b. Collision-induced dissociation of high vibrational levels populated either by multiple IR-photon absorption (**a**) or by stimulated emission pumping (**b**)

Investigations of collision processes with molecules in these selectively populated levels $|v\rangle$ yields the dependence of collision cross sections on the vibrational energy for collision-induced dissociation as well as for energy transfer into other bound levels of the molecule. Since the knowledge of this dependence is essential for a detailed understanding of the collision dynamics, a large number of theoretical and experimental papers on this subject have been published. For more information the reader is referred to some review articles and the literature given therein [8.81, 8.87, 8.93–8.95].

8.4 Spectroscopy of Reactive Collisions

A detailed understanding of reactive collisions is the basis for optimization of chemical reactions that is not dependent on "trial-and-error methods." Laser-spectroscopic techniques have opened a large variety of possible strategies to reach this goal [8.96]. Two aspects of spectroscopic investigations for reactive collisions shall be emphasized:

(a) By selective excitation of a reactant the dependence of the reaction probability on the internal energy of the reactants can be determined much more accurately than by measuring the temperature dependence of the reaction. This is because, in the latter case, internal energy and translational energy both change with temperature.
(b) The spectroscopic assignment of the reaction products and measurements of their internal energy distributions allow the identification of the different reaction pathways and their relative probabilities under definite initial conditions for the reactants.

The experimental conditions for the spectroscopy of reactive collisions are quite similar to those for the study of inelastic collisions. They range from a determination of the velocity-averaged reaction rates under selective excitation of reactants in cell experiments to a detailed state-to-state spectroscopy of reactive collisions in crossed molecular beams (Sect. 8.5). Some examples shall illustrate the state of the art:

The first experiments on state-selective reactive collisions were performed for the experimentally accessible reactions

$$\begin{aligned} &\mathrm{Ba} + \mathrm{HF}(v = 0, 1) \rightarrow \mathrm{BaF}(v = 0{-}12) + \mathrm{H}\,, \\ &\mathrm{Ba} + \mathrm{CO_2} \rightarrow \mathrm{BaO} + \mathrm{CO}\,, \\ &\mathrm{Ba} + \mathrm{O_2} \rightarrow \mathrm{BaO} + \mathrm{O}\,, \end{aligned} \tag{8.31}$$

where the internal state distribution $N(v'', J'')$ of the reaction products was measured by LIF in dependence on the vibrational energy of the halogen molecule [8.97, 8.98].

The development of new infrared lasers and of sensitive infrared detectors has allowed investigations of reactions where the reaction-product molecules have known infrared spectra but do not absorb in the visible. An example is

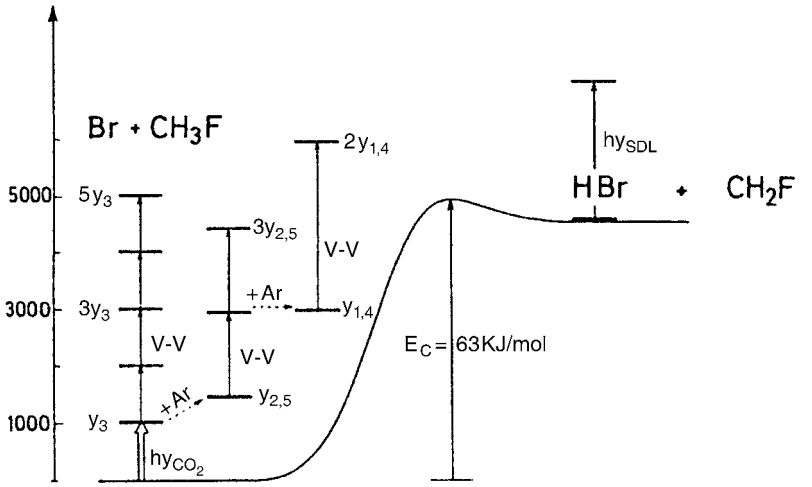

Fig. 8.21. Term diagram of the endothermic reaction $Br + CH_3F^*(v^3) \rightarrow HBr + CH_2F$ [8.99]

the endothermic reaction

$$Br + CH_3F(\nu_3) \rightarrow HBr + CH_2F\,, \tag{8.32}$$

where the CF stretching vibration ν_3 of CH_3F is excited by a CO_2 laser [8.99]. The reaction probability increases strongly with increasing internal energy of CH_3F. If a sufficiently large concentration of excited $CH_3F(\nu_3)$ molecules is reached, energy-pooling collisions

$$CH_3F^*(\nu_3) + CH_3F^*(\nu_3) \rightarrow CH_3F^{**}(2\nu_3) + CH_3F\,, \tag{8.33}$$

result in an increase of E_{vib} in one of the collision partners. The term diagram relevant for (8.32) is shown in Fig. 8.21. If the sum of internal plus kinetic energy is larger than the reaction barrier, excited product molecules may appear that can be monitored by their infrared fluorescence.

A typical experimental arrangement for such investigations is depicted in Fig. 8.22. In a flow system, where the reactive collisions take place, the levels (v, J) of the reactant molecules are selectively excited by a pulsed infrared laser. The time-dependent population of excited levels in the reactants or the product molecules are monitored through their fluorescence, detected by fast, cooled infrared detectors (Sect. 4.5).

A longstanding controversy existed on the detailed reaction mechanism of the elementary exchange reaction of hydrogen

$$H_a + H_bH_c \rightarrow H_aH_b + H_c\,, \tag{8.34a}$$

where accurate ab initio calculations of the H_3 potential surface have been performed. The experimental test of theoretical predictions is, however, very

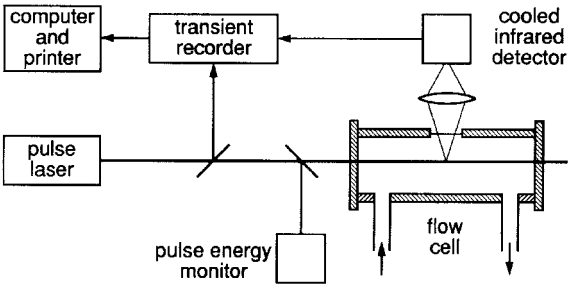

Fig. 8.22. Experimental arrangement for studies of infrared LIF in chemical reactions with spectral and time resolution

demanding. First, isotope substution has to be performed in order to distinguish between elastic and reactive scattering. Instead of (8.34a), the reaction

$$H + D_2 \rightarrow HD + D\,, \tag{8.34b}$$

is investigated. Second, all electronic transitions fall into the VUV range. The excitation of H or D_2 and the detection of HD or D require VUV lasers. Third, hydrogen atoms have to be produced since they are not available in bottles.

The first experiments were carried out in 1983 [8.100, 8.101]. The H atoms were produced by photodissociation of HJ molecules in an effusive beam using the fourth harmonics of Nd:YAG lasers. Since the dissociated iodine atom is found in the two fine-structure levels $I(P_{1/2})$ and $I(P_{3/2})$, two groups of H atoms with translational energies $E_{kin} = 0.55\,eV$ or $1.3\,eV$ in the center-of-mass system $H + D_2$ are produced. If the slower H atoms collide with D_2 they can reach vibrational–rotational excitation energies in the product molecule up to ($v = 1$, $J = 3$), while the faster group of H atoms can populate levels of HD up to ($v = 3$, $J = 8$). The internal-state distribution of the HD molecules can be monitored either by CARS (Sect. 3.3) or by resonant multiphoton ionization [8.100]. Because of their fundamental importance, these measurements have been repeated by several groups with other spectroscopic techniques that have improved signal-to-noise ratios [8.102].

An infrared laser-based method for investigating the nascent state distribution of the reaction products HF from the reaction $F + H_2 \rightarrow HF + H$ in crossed molecular beams under single collision conditions has been presented by the group of D.J. Nesbit [8.103]. The experimental setup (Fig. 8.23) consisted of a pulsed supersonic discharge source of F atoms, which collide with H_2 molecules in a second pulsed jet source. The product HF(v, J) is probed in the intersection region by the absorption of a single-mode tunable IR laser, where full vibration–rotation resolution can be achieved (Fig. 8.24).

Ion–molecule reactions, which play an important role in interstellar clouds and in many chemical and biological processes, have increasingly caught the attention of spectroscopists. As a recently investigated example, the charge-exchange reaction

$$N^+ + CO \rightarrow CO^+ + N\,,$$

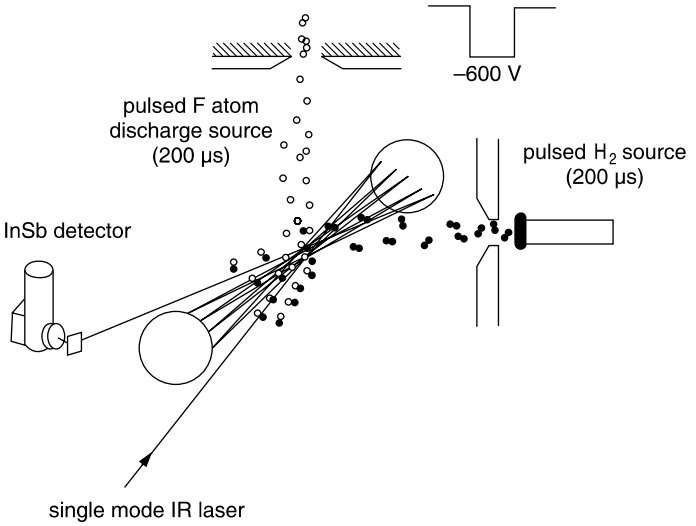

Fig. 8.23. Schematic diagram of the crossed-jet direct-absorption reactive scattering experiment. Fluorine atoms produced in a discharge pulsed jet expansion are intersected at 90° 4.5 cm downstream with a pulse of supersonically cooled H_2. Tunable single-mode IR laser light is multipassed perpendicular to the collision plane and probes HF(v, J) products by direct absorption [8.103]

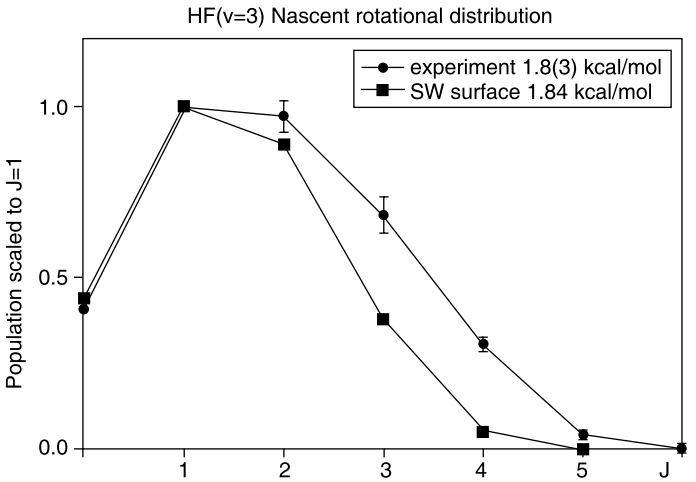

Fig. 8.24. Rotational distribution of HF($v = 3$) reaction products from the reaction $F + H_2 \rightarrow HF + H$ [8.103]

is mentioned, where the rotational distribution $N(v, J)$ of CO^+ for different vibrational levels v has been measured by infrared fluorescence (Fig. 8.25) in dependence on the kinetic energy of the N^+ ions [8.104].

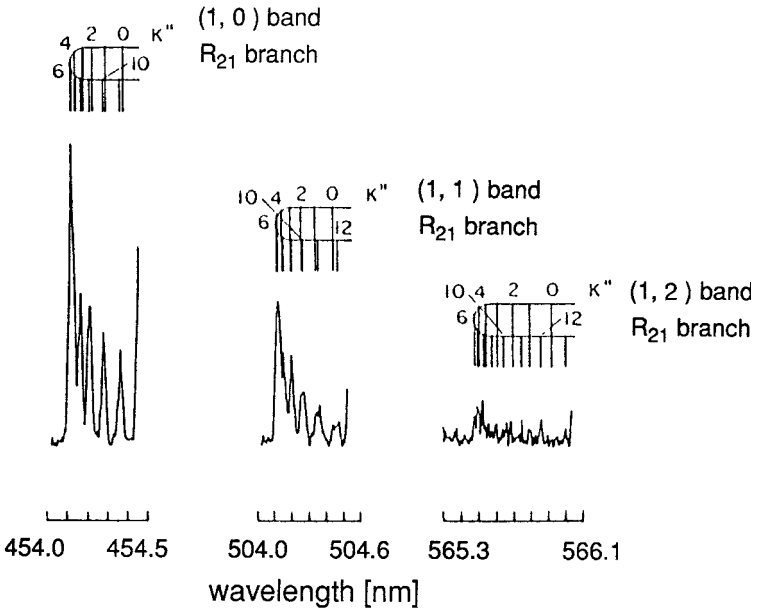

Fig. 8.25. LIF spectrum of the R_{21} band heads of CO^+ ($v = 0, 1, 2$) formed by the charge-exchange reaction $N^+ + CO \rightarrow N + CO^+$ [8.104]

Photochemical reactions are often initiated by direct photodissociation or by collision-induced dissociation of a laser-excited molecule, where radicals are formed as intermediate products, which further react by collisions. The dynamics of photodissociation after excitation of the parent molecule by a UV laser has therefore been studied thoroughly [8.105]. While the first experiments were restricted to measurements of the internal-state distribution of the dissociation products, later more refined arrangements also allowed the determination of the angular distribution and of the orientation of the products for different polarizations of the photodissociating laser [8.106–8.108]. The technique is illustrated by the example

$$\mathrm{ICN} \underset{248\,\mathrm{nm}}{\overset{h\nu}{\rightarrow}} \mathrm{CN} + \mathrm{I}$$

which was investigated with the apparatus depicted in Fig. 8.26. The ICN molecules are dissociated by the circularly polarized radiation of a KrF laser at $\lambda = 248\,\mathrm{nm}$. The orientation of the CN fragments is monitored through the fluorescence induced by a polarized dye laser. The dye laser is tuned through the $B\,^2\Sigma \leftarrow X\,^2\Sigma^+$ systen of CN. This circular polarization is periodically switched between σ^+ and σ^- by a photoelastic polarization modulator (PEM). The corresponding change in the fluorescence intensity is a measure of the orientation of the CN fragments [8.109].

A famous example is the photodissociation of H_2O leading to a preferentially populated Λ component of the OH fragment, which forms the basis

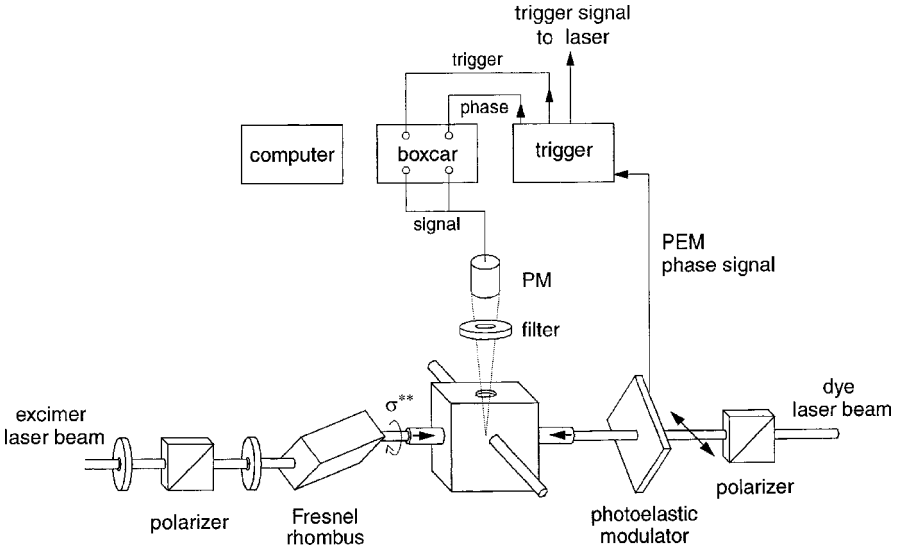

Fig. 8.26. Schematic experimental arrangement for measurements of the fragment orientation after photodissociation of the parent molecule [8.109]

of the astromonical OH maser observed in interstellar clouds [8.110]. There are many more examples of laser spectroscopy of chemical reactions, some of which can be found in [8.111–8.115].

8.5 Spectroscopic Determination of Differential Collision Cross Sections in Crossed Molecular Beams

The techniques discussed in Sects. 8.2–8.4 allowed the measurement of absolute rate constants of selected collision-induced transitions, which represent *integral* inelastic cross sections integrated over the angular distribution and averaged over the thermal velocity distribution of the collision partners. Much more detailed information on the interaction potential can be extracted from measured *differential* cross sections, obtained in crossed molecular beam experiments [8.1, 8.116, 8.117].

Assume that atoms or molecules A in a collimated beam collide with atoms or molecules B within the interaction volume V formed by the overlap of the two beams (Fig. 8.27). The number of particles A scattered per second by the angle θ into the solid angle $\mathrm{d}\Omega$ covered by the detector D is given by

$$\frac{\mathrm{d}N_\mathrm{A}(\theta)}{\mathrm{d}t}\,\mathrm{d}\Omega = n_\mathrm{A} v_\mathrm{r} n_\mathrm{B} V \frac{\mathrm{d}\sigma(\theta)}{\mathrm{d}\Omega}\,\mathrm{d}\Omega\,, \tag{8.35}$$

where n_A is the density of the incident particles A, n_B the density of particles B, v_r is the relative velocity, and $(\mathrm{d}\sigma(\theta)/\mathrm{d}\Omega)$ the differential scattering cross section. The scattering angle ϑ is related to the impact parameter b

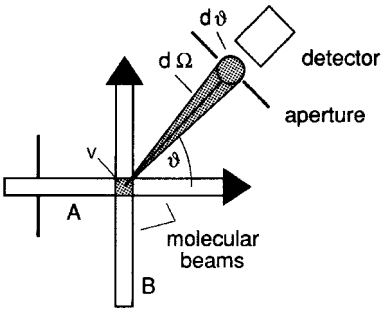

Fig. 8.27. Schematic diagram for the measurement of differential cross sections in crossed molecular beams

and the interaction potential. It can be calculated for a given potential $V(r)$ [8.118]. Differential cross sections probe definite local parts of the potential, while integral cross sections only reflect the global effect of the potential on the deflected particles, averaged over all impact parameters. We will discuss which techniques can be used to measure differential cross sections for elastic, inelastic, and reactive collisions.

With classical techniques, the energy loss of the particle A during an inelastic collision is determined by measuring its velocity before and after the collision with velocity selectors or by time-of-flight measurements [8.33]. Since the velocity resolution $\Delta v/v$ and therefore the minimum detectable energy loss ΔE_{kin} is restricted by technical limitations, this method can be applied to only a limited number of real problems.

For polar molecules with an electric dipole moment, Rabi spectrometers with electrostatic quadrupole deflection fields offer the possibility to detect rotationally inelastic collisions since the focusing and deflecting properties of the quadrupole field depend on the quantum state $|J, M\rangle$ of a polar molecule. This technique is, however, restricted to molecules with a large electric dipole moment and to small values of the rotational quantum number J [8.118].

Applications of laser-spectroscopic techniques can overcome many of the above-mentioned limitations. The energy resolution is higher by several orders of magnitude than that for time-of-flight measurements. In principle, molecules in arbitrary levels $|v, J\rangle$ can be investigated, as long as they have absorption transitions within the spectral range of available lasers. The essential progress of laser spectroscopy is, however, due to the fact that besides the scattering angle θ, the initial and final quantum states of the scattered particle A can also be determined. In this respect, laser spectroscopy of collisions in crossed beams represents the *ideal complete scattering experiment* in which all the relevant parameters are measured.

The technique is illustrated by Fig. 8.28. A collimated supersonic beam of argon, which contains Na atoms and Na_2 molecules, is crossed perpendicularly with a noble gas beam [8.119]. Molecules of Na_2 in the level $|v''_m J''_m\rangle$ that have been scattered by the angle ϑ are monitored by a *quantum-state-specific detector*. It consists of a cw dye laser focused into a spot behind the aperture A and tuned to the transition $|v''_m, J''_m\rangle \rightarrow |v'_j, J'_j\rangle$, and an optical system

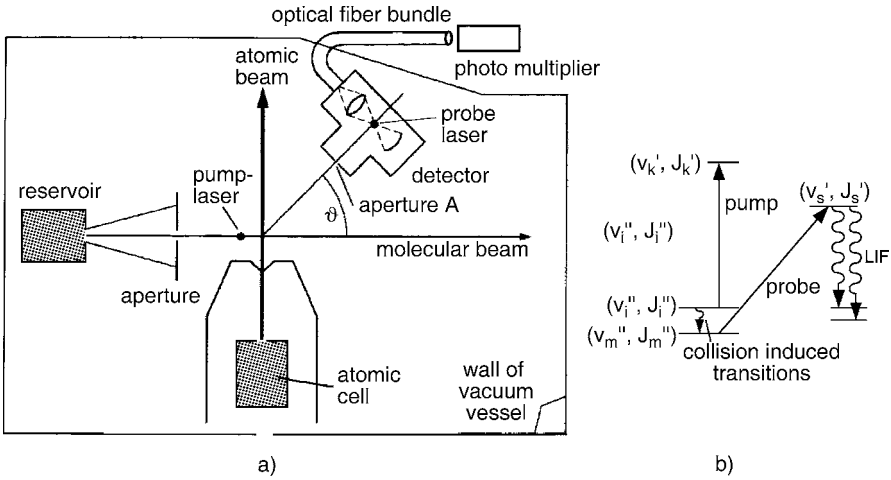

Fig. 8.28. (**a**) Experimental arrangement for the spectroscopic determination of state-to-state differential cross sections [8.120]. (**b**) Level scheme for pump-probe experiment

of a mirror and lens, which collects the LIF through an optical fiber bundle onto a photomultiplier. The entire detector can be turned around the scattering center.

We define θ as the scattering angle in the center-of-mass system (while ϑ is that in the laboratory system). The detected intensity of the LIF is a measure of the scattering rate $[\mathrm{d}N(v''_m, J''_m, \theta)/\mathrm{d}t]\mathrm{d}\Omega$ which has two contributions:

(a) The elastically scattered molecules $(v''_m, J''_m) \rightarrow (v''_m, J''_m, \theta)$, and
(b) the sum of all inelastically scattered molecules which have suffered collision-induced transitions $\sum_n [(v''_n, J''_n) \rightarrow (v''_m, J''_m)]$.

In order to select molecules with definite initial and final states, an OODR method is used (Sect. 5.4). Shortly before they reach the scattering volume, the molecules pass through the beam of a pump laser that induces transitions $(v''_i, J''_i) \rightarrow (v'_k, J'_k)$ and depletes the lower level (v''_i, J''_i) by optical pumping (Fig. 8.29). If the scattering rate is measured by the detector alternately with the pump laser on and off, the difference of the two signals just gives the contribution of those molecules with initial state (v''_i, J''_i), final state (v''_m, J''_m), and scattering angle θ [8.120].

Since the scattering angle θ is related to the impact parameter b, the experiment indicates which impact parameters contribute preferentially to collision-induced vibrational or rotational transitions, and how the transferred angular momentum ΔJ depends on impact parameters, initial state (v''_i, J''_i), and collision partner B [8.121]. In Fig. 8.30 some differential cross sections $\sigma(\theta)$ for inelastic $Na_2 + Ne$ collisions are plotted versus the scattering angle θ. Note that angular momentum transfer of up to $\Delta J = 55\hbar$ has been observed. The analysis of the measured data yields very accurate interaction potentials.

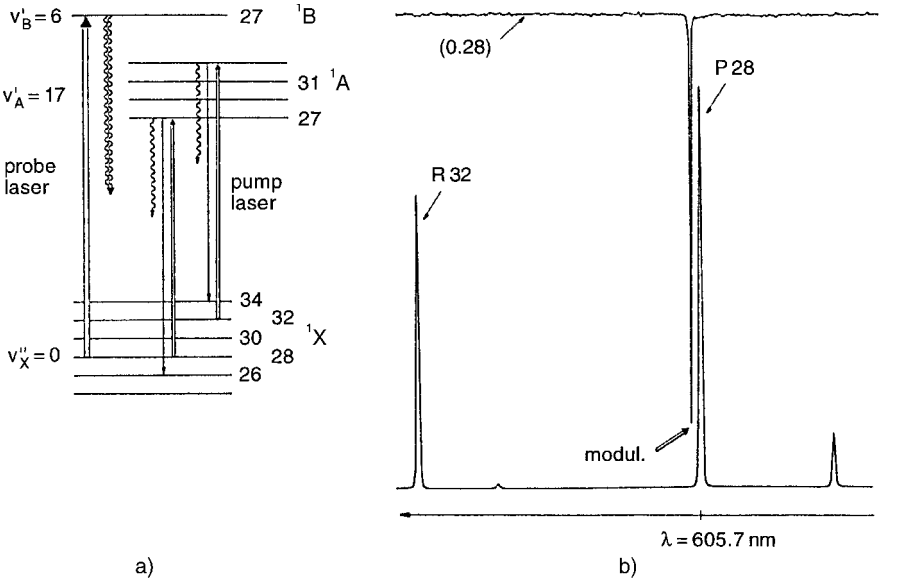

Fig. 8.29. (**a**) Level diagram of Na_2 for optical depletion of the levels $(v'', J'') = (0, 28)$ and optical probing of collisionally populated levels $(v'', J'' + \Delta J)$. (**b**) The measured spectrum in the right part gives the experimental proof that a level (v'', J'') can be completely depleted by optical pumping. The *lower* spectrum shows the pump laser-induced fluorescence I_{Fl} (L1) when the laser L1 is tuned, the *upper* trace the probe laser-induced fluorescence, where the probe laser was stabilized onto the transition $X(v'' = 0, J'' = 28) \rightarrow B(v' = 6, J' = 27)$. When the pump laser is tuned over the transition starting from $X(v'' = 0, J'' = 28)$ the probe laser-induced fluorescence drops nearly to zero. The *lower* spectrum has been shifted by 2 mm to the right [8.121]

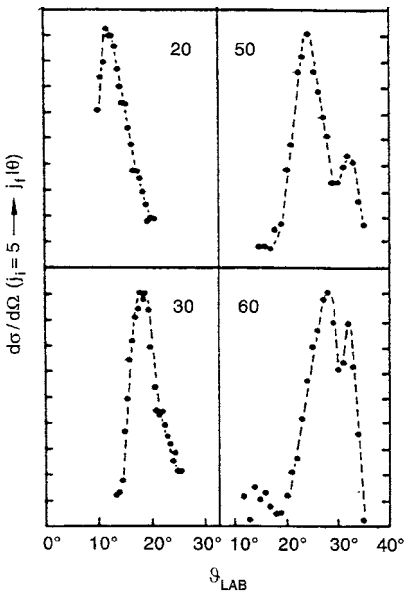

Fig. 8.30. Differential cross sections for collision-induced rotational transitions $[J_i = 5 \rightarrow J_f = J_i + \Delta J]$ in $Na_2 + Ne$ collisions for different values of J_f versus the scattering angle ϑ in the laboratory system [8.121]

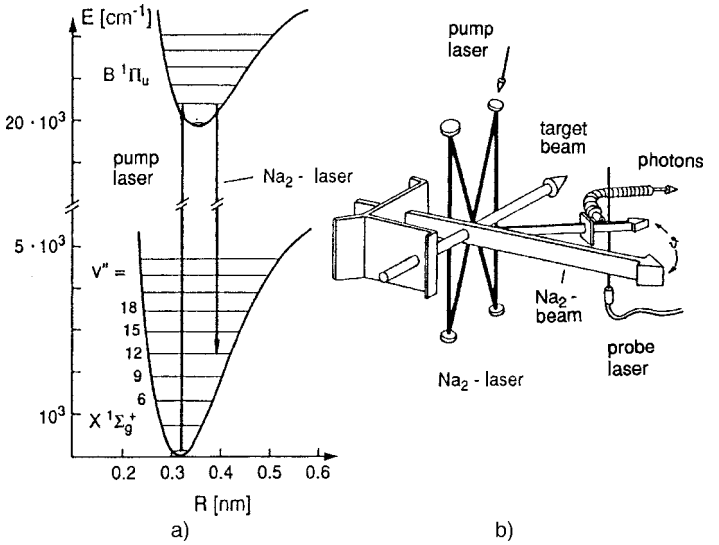

Fig. 8.31a,b. Selective pumping of a high vibrational level (v, J) by stimulated emission pumping in Na_2 with a Na_2 dimer laser: (**a**) level scheme; (**b**) experimental realization [8.123]

Of particular interest is the dependence of collision cross sections on the vibrational state, since the probability of inelastic and reactive collisions increases with increasing vibrational excitation [8.122]. Stimulated emission pumping or STIRAP (see Sect. 7.3) before the scattering center allows a large population transfer into selected, high vibrational levels of the electronic ground state. For some molecules, such as Na_2 or I_2, an elegant realization of this technique is based on a molecular beam dimer laser [8.123], which uses the molecules in the primary beam as an active medium pumped by an argon laser or a dye laser (Fig. 8.31). Threshold pump powers below 1 mW (!) could indeed be achieved.

Optical pumping also allows measurements of differential cross sections for collisions where one of the partners is electronically excited. The interaction potential $V(A^*, B)$ could be determined in this way for alkali–noble gas partners, which represent exciplexes since they are bound in an excited state but dissociate in the unstable ground state. One example is the investigation of K + Ar collision partners [8.124]. In the crossing volume of a potassium beam and an argon beam, the potassium atoms are excited by a cw dye laser into the $4\,P_{3/2}$ state. The scattering rate for K atoms is measured versus the scattering angle θ with the pump laser on and off. The signal difference yields the contribution of the excited atoms to the elastic scattering if the fraction of excited atoms can be determined, which demands a consideration of the hyperfine structure. In order to reach the maximum concentration of excited K atoms, either a single-mode circularly polarized dye laser must be used, which is tuned to the transition $F'' = 2 \rightarrow F' = 3$ between selected hfs components, or a broad-band laser, which pumps all allowed hfs transitions simultaneously.

An example of measurements of *inelastic* collisions between excited atoms A* and molecules M in crossed beams is the experiment by Hertel et al. [8.125], where laser-excited Na*(3P) atoms collide with molecules such as N_2 or CO and the energy transfer

$$A^*M(v'' = 0) \rightarrow A + M(v'' > 0) + \Delta E_{kin} , \tag{8.36}$$

is studied. If the scattering angle θ and the velocity of the scattered Na atoms are measured, kinematic considerations (energy and momentum conservation) allow the determination of the fraction of the excitation energy that is converted into internal energy of M and that is transferred into kinetic energy ΔE_{kin}. The experimental results represent a crucial test of ab initio potential surfaces $V(r, \theta, \phi)$ for the interaction potential $Na^* - N_2$ ($v = 1, 2, 3, ...$) [8.126].

Scattering of electrons, fast atoms, or ions with laser-excited atoms A* can result in elastic, inelastic, or superelastic collisions. In the latter case, the excitation energy of A* is partly converted into kinetic energy of the scattered particles. Orientation of the excited atoms by optical pumping with polarized lasers allows investigations of the influence of the atomic orientation on the differential cross sections for $A^* + B$ collisions, which differs for collisions with electrons or ions from the case of neutral atoms [8.127]. An example of the measurement of differential cross sections of the reactive collisions $Na^* + HF$ is given in [8.128].

Measurements of differential cross-sections for reactive collisions allow the determination of reaction rates and the internal state distributions of reaction products as well as their dependence on scattering angle and internuclear distances during the reaction. This gives a much more detailed insight into the time sequence of the reaction during the approach of the reactants. Therefore, many experiments have been performed where the quantum states of the reactants have been selected by laser excitation, the product state distribution by LIF and the scattering angle by using crossed beam arrangements and angular resolved detection. One example is the observation of resonances in the cross-section for the reaction $F + HD \rightarrow FH + D$ or $FD + H$, where a virtual level of the transition state opens up the specific reaction channel for the formation of $HF(v = 3)$ in a specific quantum state [8.129].

From the measured angular distribution of the reaction products IF formed in the reaction $F + C_2H_5I \rightarrow IF + C_2H_5$, it can be concluded that the transition complex during this reaction has a lifetime of at least 2–3 rotational periods [8.130].

8.6 Photon-Assisted Collisional Energy Transfer

If two collision partners A and M absorb a photon $h\nu$ at a relative distance R_c, one of the partners may remain in an excited state after the collision:

$$A + M + h\nu \rightarrow A^* + M . \tag{8.37}$$

This reaction can be regarded as the three step process:

$$A + M \rightarrow (AM)\,, \tag{8.38}$$

$$(AM) \rightarrow h\nu \rightarrow (AM)^*\,, \tag{8.39}$$

$$(AM)^* \rightarrow A^* + M\,. \tag{8.40}$$

The two collision partners form a collision complex that is excited by absorption of the photon $h\nu$ at a relative distance R_c, where the energy difference $\Delta E = E(AM)^* - E(AM)$ between the two potential curves just equals the photon energy $h \cdot \nu$ (Fig. 8.32a) and the Franck–Condon factor has a maximum value [8.131]. This complex decays after a short time into $A^* + M$.

If the potential is not monotonic, there are generally two trajectories with different impact parameters that lead to the same deflection angle θ in the center of mass system (Fig. 8.32b).

In a similar way collisions with excited atoms can be studied. The energy transfer by inelastic collisions between excited atoms A^* and ground-state atoms B

$$A^* + B \rightarrow B^* + A + \Delta E_{kin}\,, \tag{8.41}$$

is governed by the conservation of energy and momentum. The energy difference $\Delta E_{int} = E(A^*) - E(B^*)$ is transferred into kinetic energy ΔE_{kin} of the collision partners. For $\Delta E_{kin} \gg KT$, the cross section σ for the reaction (8.41) becomes very small, while for near-resonant collisions ($\Delta E_{kin} \ll KT$), σ may exceed the gas kinetic cross section by several orders of magnitude.

If such a reaction (8.41) proceeds inside the intense radiation field of a laser, a photon may be absorbed or emitted during the collision, which may help to satisfy energy conservation for small ΔE_{kin} even if ΔE_{int} is large.

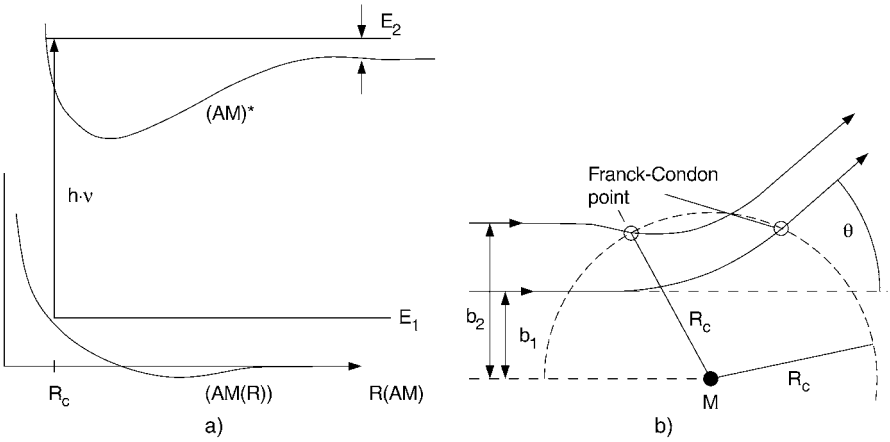

Fig. 8.32a,b. Schematic diagram of "optical collisions": (**a**) potential curves of ground and excited state of the collision complex; (**b**) classical trajectories in the center-of-mass system for two different impact parameters b_1, b_2

Instead of (8.41), the reaction is now

$$A^* + B \pm \hbar\omega \rightarrow B^* + A + \Delta E_{kin} \,. \tag{8.42}$$

For a suitable choice of the photon energy $\hbar\omega$, the cross section for a nonresonant reaction (8.41) can be increased by many orders of magnitude through the help of the photon, which makes the process near resonant. Such *photon-assisted* collisions will be discussed in this section.

In the *molecular* model of Fig. 8.33a the potential curves $V(R)$ are considered for the collision pairs $A^* + B$ and $A + B^*$. At the critical distance R_c the energy difference $\Delta E = V(AB^*) - V(A^*B)$ may be equal to $\hbar\omega$. Resonant absorption of a photon by the collision pair $A^* + B$ at the distance R_c results in a transition into the upper potential curve $V(AB^*)$, which separates into $A + B^*$. The whole process (8.42) then leads to an energy transfer from A^* to B^*, where the initial and final kinetic energy of the collision partners depends on the slope dV/dR of the potential curves and the internuclear distance R_c where photon absorption takes place.

If we start with $A + B^*$ the inverse process of stimulating photon emission will result in a transition from the upper into the lower potential, which means an energy transfer from B^* to A^* for the separated atoms.

For the experimental realization of such photon-assisted collisional energy transfer one needs two lasers: the pump laser L1 excites the atoms A into the excited state A^* and the transfer laser L2 induces the transition between the two potential curves $V(A^*B) \rightarrow V(AB^*)$.

In the *atomic model* (Fig. 8.33b, often called the *dressed-atom model*) [8.132] the excited atom A^* absorbes a photon $\hbar\omega$ of the transfer laser, which excites A^* further into a *virtual state* $A^* + \hbar\omega$ that is near resonant with the excited state of B^*. The collisional energy transfer $A^* + \hbar\omega \rightarrow B^* + \Delta E_{kin}$

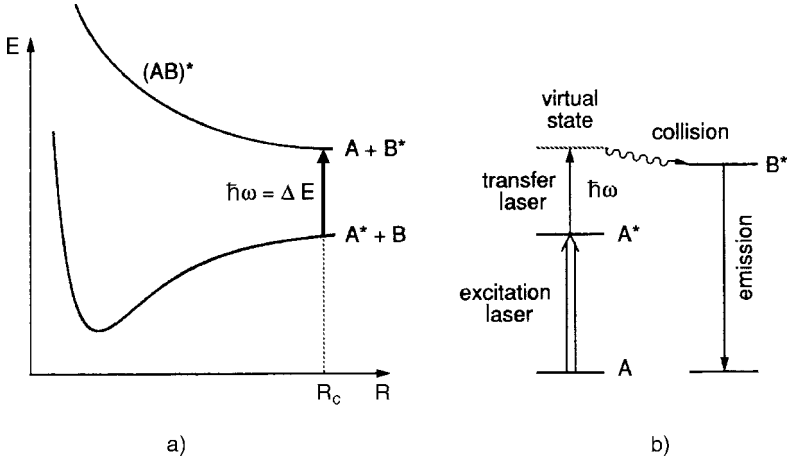

Fig. 8.33a,b. Photon-assisted collisional energy transfer: (**a**) molecular model; (**b**) dressed-atom model

with $\Delta E_{\text{kin}} \ll \hbar\omega$ then proceeds with a much higher probability than the off-resonance process without photon absorption [8.133].

The first experimental demonstration of photon-assisted collisional energy transfer was reported by Harris and coworkers [8.134], who studied the process

$$\begin{aligned} \mathrm{Sr}^*(5\,^1\mathrm{P}) + \mathrm{Ca}(4\,^1\mathrm{S}) + \hbar\omega &\rightarrow \mathrm{Sr}(5\,^1\mathrm{S}) + \mathrm{Ca}(5^1\mathrm{D})\,, \\ &\rightarrow \mathrm{Sr}(5\,^1\mathrm{S}) + \mathrm{Ca}(4p^2\,^1\mathrm{S})\,. \end{aligned}$$

The corresponding term diagram is depicted in Fig. 8.34. The strontium atoms are excited by a pulsed pump laser at $\lambda = 460.7\,\mathrm{nm}$ into the level $5s5p\,^1\mathrm{P}_1^0$. During the collision with a Ca atom in its ground state the collision pair $\mathrm{Sr}(5\,^1\mathrm{P}_1^0)$–$\mathrm{Ca}(4\,^1\mathrm{S})$ absorbs a photon $\hbar\omega$ of the transfer laser at $\lambda = 497.9\,\mathrm{nm}$. After the collision the excited $\mathrm{Ca}^*(4p^2\,^1\mathrm{S})$ atoms are monitored through their fluorescence at $\lambda = 551.3\,\mathrm{nm}$.

It is remarkable that the transitions $4s^2\,^1\mathrm{S}_1 \rightarrow 4p^2\,^1\mathrm{S}$ and $4s^2\,^1\mathrm{S} \rightarrow 4p^2\,^1\mathrm{D}$ of the Ca atom do not represent allowed dipole transitions and are therefore forbidden for the isolated atom. Regarding the photon-absorption probability, the absorption by a collision pair with subsequent energy transfer to the atom is therefore called *collision-induced absorption* or collision-aided radiative excitation [8.135], where a *dipole-allowed* transition of the molecular collision pair A*B or AB* takes place. The molecular transition has a dipole transition moment $\mu(R)$ that depends on the internuclear separation R(A*B) and that approaches zero for $R \rightarrow \infty$ [8.136]. It is caused by the induced dipole–dipole interaction from the polarizability of the collision partners.

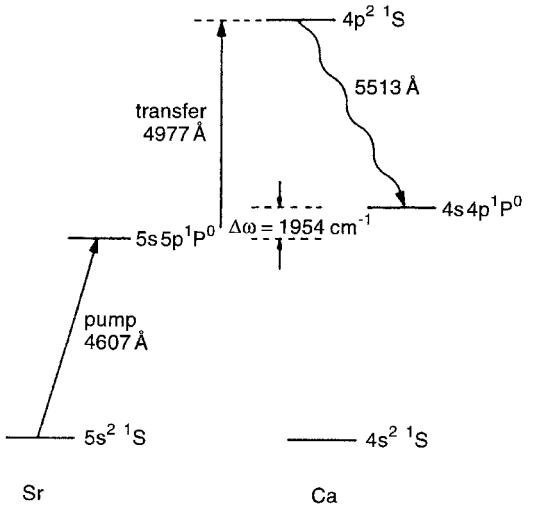

Fig. 8.34. Term diagram for photon-assisted collisional energy transfer from $\mathrm{Sr}^*(^1\mathrm{P}^0)$ to $\mathrm{Ca}(4p^2\,^1\mathrm{S})$ [8.134]

Such collision-induced absorption of radiation is important not only for the initiation of chemical reactions (Sect. 10.2), but also plays an important role in the absorption of infrared radiation in planetary atmospheres and interstellar molecular clouds. By the formation of H_2–H_2 collision pairs, for instance, vibration–rotational transitions within the electronic ground state of H_2 become allowed although they are forbidden in the isolated homonuclear H_2 molecule [8.137, 8.138].

An interesting aspect of collision-aided radiative excitation is its potential for optical cooling of vapors. Since the change in kinetic energy of the collision partners per absorbed photon can be much larger than that transferred by photon recoil (Sect. 9.1), only a few collisions are necessary for cooling to low temperatures compared with a few thousand for recoil cooling [8.135].

Detailed investigations of the transfer cross section and its dependence on the wavelength λ_2 of the transfer laser L2 have been performed by Toschek and coworkers [8.139], who studied the reaction $Sr(5s5p) + Li(2s) + \hbar\omega \rightarrow Sr(5s^2) + Li(4d)$. The experimental setup is shown in Fig. 8.35. A mixture of strontium and lithium vapors is produced in a heat pipe [8.22]. The beams of two dye lasers pumped by the same N_2 laser are superimposed and focused into the center of the heat pipe. The first laser L1 at $\lambda_1 = 407\,\text{nm}$ excites the Sr atoms. The pulse of the second laser L2 is delayed by a variable time interval Δt and its wavelength λ_2 is tuned around $\lambda_1 = 700\,\text{nm}$. The intensity $I_{Fl}(\lambda_2, \Delta t)$ of the fluorescence emitted by the excited Li* atoms is monitored in the transition $Li(d\,^2D \rightarrow 2p\,^2P)$ at $\lambda = 610\,\text{nm}$ as a function of the wavelength λ_2 and the delay time Δt. For the resonance case λ_2^{res} (that is, $\Delta E_{kin} = 0$ in (8.42)) energy transfer cross sections up to $\sigma_T > 2 \times 10^{-13}\, I \cdot \text{cm}^2$ (where I is measured in MW/cm^2) have been determined.

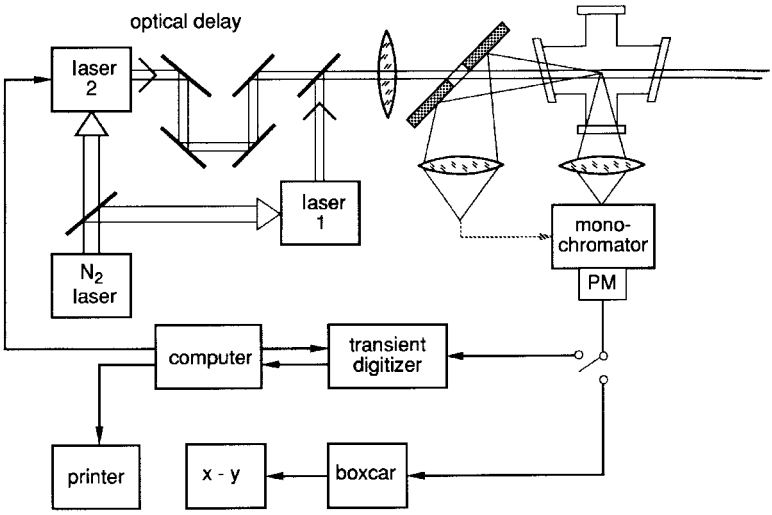

Fig. 8.35. Experimental setup for studies of photon-assisted collisional energy transfer [8.139]

For sufficiently high intensities I of the transfer laser, the photon-assisted collisional transfer cross sections σ_T exceed the gas-kinetic cross sections $\sigma \approx 10^{-15}\,\mathrm{cm}^2$ by 2–3 orders of magnitude.

From the angular distribution of $K(^2P)$ atoms formed in the optical collision

$$K((4s)^2\,{}^2P) + Ar + h\nu \rightarrow K((4p)^2\,{}^2P) + Ar,$$

the repulsive potential curves of the unstable molecule $KAr(X^2\Sigma)$ and $KAr(B^2\Sigma)$ could be obtained with an accuracy of about 1% [8.140].

Example 8.1.

For saturation of the pump transition even moderate intensities ($I_p < 10^3\,\mathrm{kW/cm}^2$) are sufficient (Sect. 2.1). Assume an output power of 50 kW of the transfer laser L2 and a beam diameter of 1 mm in the focal plane, which yields $I_{transf} = 6.7\,\mathrm{MW/cm}^2$, energy transfer cross sections of $\sigma_T \approx 1.3 \times 10^{-12}\,\mathrm{cm}^2$, which is about 1000 times larger than the gas-kinetic cross section. The energy transfer $R_T = \sigma n \bar{v} h\nu_T$, where n is the density of collision partners, colliding with the excited atoms. With $n = 10^{16}\,\mathrm{cm}^3$, $\bar{v} = 10^5\,\mathrm{cm/s}$ and $h\nu_T = 2\,\mathrm{eV}$, we obtain $R_T = 10^9\,\mathrm{eV/s}$.

Further information on this interesting field and its various potential application can be found in [8.141, 8.142]. A compendium of data on Atomic Collisions up to 1994 is compiled in [8.143]. A chronicle of fifty years on the dynamics of molecular processes is given in [8.144].

Problems

8.1 Assume an inelastic cross section of $\sigma^{inel} = 10^{-15}\,\mathrm{cm}^2$ for collisions between excited atoms A* and partners B, and a velocity-changing cross section $\sigma_v(\Delta v) = \sigma_0 \exp(-\Delta v^2/\langle v^2\rangle)$ for velocity changes Δv of atom A. Discuss for $\sigma_0 = 10^{-14}\,\mathrm{cm}^2$ the line profile of the Lamb dip in the transition $A \rightarrow A^*$ if the radiative lifetime is $\tau_{rad} = 10^{-8}\,\mathrm{s}$, the pressure of partners B is 1 mbar, the temperature $T = 300\,\mathrm{K}$, the saturation parameter $S = 1$, and the reduced mass $\mu(AB) = 40\,\mathrm{AMU}$.

8.2 The effective lifetime of an excited molecular level is $\tau_{eff}(p = 5\,\mathrm{mbar}) = 8 \times 10^{-9}\,\mathrm{s}$ and $\tau_{eff}(p = 1\,\mathrm{mbar}) = 12 \times 10^{-9}\,\mathrm{s}$ for molecules with the mass $M = 43\,\mathrm{AMU}$ in a gas cell with argon buffer gas at $T = 500\,\mathrm{K}$. Calculate the radiative lifetime, the collision-quenching cross section, and the homogeneous linewidth $\Delta\nu(p)$.

8.3 A single-mode laser beam with a Gaussian profile ($w = 1\,\mathrm{mm}$) and a power of 10 mW, tuned to the center ω_0 of the sodium line ($3\,{}^2S_{1/2} \rightarrow 3\,{}^2P_{1/2}$) passes through a cell containing sodium vapor at $p = 10^{-3}\,\mathrm{mbar}$

at a temperature of 450 K. The absorption cross section is $\sigma_{\text{abs}} = 5 \times 10^{-11}\,\text{cm}^2$, the natural linewidth is $\delta\nu_n = 10\,\text{MHz}$, the collision cross section $\sigma_{\text{col}} = 10^{-12}\,\text{cm}^2$ and the Doppler width $\delta\nu_{\text{D}} = 1\,\text{GHz}$. Calculate the saturation parameter S, the absorption coefficient $\alpha_s(\omega_0)$, and the mean density of ground-state and excited atoms that collide in an energy-pooling collision with $\sigma_{\text{ep}} = 3 \times 10^{-14}\,\text{cm}^2$. Which Rydberg levels are accessible by energy-pooling collisions $\text{Na}^*(3P) + \text{Na}^*(3P)$ if the relative kinetic energy is $E_{\text{kin}} \leq 0.1\,\text{eV}$?

8.4 A square-wave chopped cw laser depopulates the level (v_i'', J_i'') in the electronic ground state of the molecule M with $m = 40\,\text{AMU}$. What is the minimum chopping period T to guarantee quasi-stationary conditions for level $|i\rangle$ and its neighboring levels $|J_i \pm \Delta J\rangle$, if the total refilling cross section of level $|i\rangle$ is $\sigma = 10^{-14}\,\text{cm}^2$ and the individual cross sections $\sigma_{ik} = (3 \times 10^{-16}\,\Delta\,\text{J})\,\text{cm}^2$ for transitions between neighboring levels $|J\rangle$ and $|J \pm \Delta J\rangle$ of the same vibrational level at a pressure of 1 mbar and a temperature of 300 K?